Lithospheric structure of the Aegean obtained from P and S receiver functions

F. Sodoudi,[1] R. Kind,[1,2] D. Hatzfeld,[3] K. Priestley,[4] W. Hanka,[1] K. Wylegalla,[1] G. Stavrakakis,[5] A. Vafidis,[6] H.-P. Harjes,[7] and M. Bohnhoff[1]

Received 6 July 2005; revised 2 August 2006; accepted 8 September 2006; published 27 December 2006.

[1] Combined P and S receiver functions from seismograms of teleseismic events recorded at 65 temporary and permanent stations in the Aegean region are used to map the geometry of the subducted African and the overriding Aegean plates. We image the Moho of the subducting African plate at depths ranging from 40 km beneath southern Crete and the western Peloponnesus to 160 km beneath the volcanic arc and 220 km beneath northern Greece. However, the dip of the Moho of the subducting African plate is shallower beneath the Peloponnesus than beneath Crete and Rhodes and flattens out beneath the northern Aegean. Observed P-to-S conversions at stations located in the forearc indicate a reversed velocity contrast at the Moho boundary of the Aegean plate, whereas this boundary is observed as a normal velocity contrast by the S-to-P conversions. Our modeling suggests that the presence of a large amount of serpentinite (more than 30%) in the forearc mantle wedge, which generally occurs in the subduction zones, may be the reason for the reverse sign of the P-to-S conversion coefficient. Moho depths for the Aegean plate show that the southern part of the Aegean (crustal thickness of 20–22 km) has been strongly influenced by extension, while the northern Aegean Sea, which at present undergoes the highest crustal deformation, shows a relatively thicker crust (25–28 km). This may imply a recent initiation of the present kinematics in the Aegean. Western Greece (crustal thickness of 32–40 km) is unaffected by the recent extension but underwent crustal thickening during the Hellenides Mountains building event. The depths of the Aegean Moho beneath the margin of the Peloponnesus and Crete (25–28 and 25–33 km, respectively) show that these areas are also likely to be affected by the Aegean extension, even though the Cyclades (crustal thickness of 26–30 km) were not significantly involved in this episode. The Aegean lithosphere-asthenosphere boundary (LAB) mapped with S receiver functions is about 150 km deep beneath mainland Greece, whereas the LAB of the subducted African plate dips from 100 km beneath Crete and the southern Aegean Sea to about 225 km under the volcanic arc. This implies a thickness of 60–65 km for the subducted African lithosphere, suggesting that the Aegean lithosphere was not significantly affected by the extensional process associated with the exhumation of metamorphic core complexes in the Cyclades.

Citation: Sodoudi, F., R. Kind, D. Hatzfeld, K. Priestley, W. Hanka, K. Wylegalla, G. Stavrakakis, A. Vafidis, H.-P. Harjes, and M. Bohnhoff (2006), Lithospheric structure of the Aegean obtained from P and S receiver functions, *J. Geophys. Res.*, *111*, B12307, doi:10.1029/2005JB003932.

1. Introduction

[2] The crustal and upper mantle structures of the Aegean are the result of a complex tectonic history that started probably during the late Cretaceous [e.g., *McKenzie*, 1972] and resulted in the subduction of Africa beneath Eurasia, the building of mountain belts and the creation of stretched regions. The present-day kinematics and deformation are reasonably well known because of the large number of GPS measurements covering the Aegean [e.g., *Le Pichon et al.*, 1995; *Reilinger et al.*, 1997; *McClusky et al.*, 2000]. However, the present-day kinematics is certainly different from that of the past, as is attested by the large amount of

[1]GeoForschungsZentrum Potsdam, Potsdam, Germany.
[2]Also at Department of Geophysics, Freie Universität Berlin, Berlin, Germany.
[3]Laboratoire des Geophysique Interne et Tectonophysique, Grenoble, France.
[4]Bullard Laboratory, Cambridge, UK.
[5]National Observatory of Athens, Athens, Greece.
[6]Department of Mineral Resources Engineering, Technical University of Chania, Chania, Greece.
[7]Department of Geosciences, Ruhr-University Bochum, Bochum, Germany.

Copyright 2006 by the American Geophysical Union.
0148-0227/06/2005JB003932$09.00

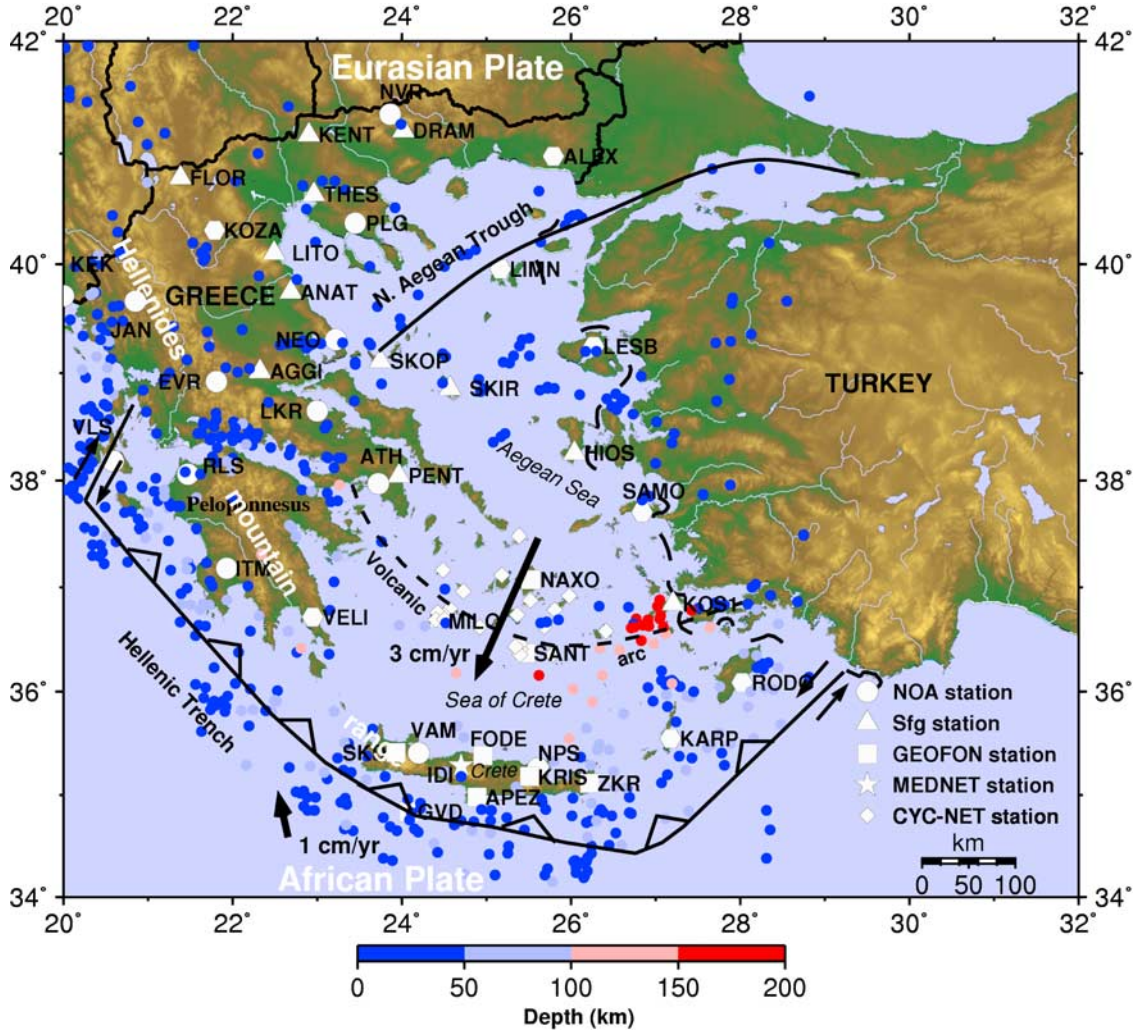

Figure 1. Location map of the seismological stations used in this study. Hexagons denote the location of both NOA and sfg stations. Small circles indicate epicenters of the shallow and intermediate ($m_b \geq 4.5$) depth earthquakes [*Engdahl et al.*, 1988]. Locations of the Hellenic trench and the North Aegean Trough are drawn with black solid lines. Dashed line denotes location of the volcanic arc. The arrows indicate the direction of the motion relative to Eurasia [*McClusky et al.*, 2000].

rotation that the Hellenic arc experienced since the Oligocene [*Kissel and Laj*, 1988].

[3] During the past 3–5 million years, the Aegean has been moving to the southwest with respect to Eurasia at an average velocity of ~3.5 cm/yr across the Hellenic trench [e.g., *McKenzie*, 1972; *Jackson and McKenzie*, 1988; *McClusky et al.*, 2000] and has lead to the northward subduction of the African lithosphere beneath the Aegean [*Papazachos and Comninakis*, 1969]. Relative to Eurasia the African lithosphere is converging at a rate of ~1 cm/yr [*DeMets et al.*, 1990], whereas the Aegean is extending at a rate of ~3 cm/yr (Figure 1). To a first approximation, the motion of the Aegean relative to Eurasia can be described as the superposition of a rigid rotation of Anatolia and the local extension that affects the Aegean probably related to the slab retreat [*Le Pichon and Angelier*, 1979]. Data from satellite geodesy [*Kahle et al.*, 1998], seismicity [*Ekström and England*, 1989; *Hatzfeld et al.*, 1997; *Jackson et al.*, 1994], sediments infillings and deformation [*Mascle and Martin*, 1990; *Mercier et al.*, 1989] all show that at present, the crustal deformation is highest in the northern Aegean Sea along the North Aegean Trough and is also concentrated in grabens located west and east of the Aegean region [*Armijo et al.*, 1996].

[4] Details of earlier episodes of Aegean deformation are less well known. It is likely that prior to the Oligo-Miocene time, the slow convergence between Africa and Eurasia was accommodated by the northward dipping subduction of the African lithosphere along an E-W trending boundary. During the Oligo-Miocene time, extension started in the southern Aegean as attested by the creation of deep basins [*Mascle and Martin*, 1990] and the exhumation of metamorphic core complexes mostly in the Cyclades [e.g., *Gautier and Brun*, 1994]. This earlier mode of extension was greatest in the Sea of Crete where it reaches a factor of two [*McKenzie*, 1978; *Angelier et al.*, 1982], and it is responsible for the curvature of the Hellenic arc. This extension is consistent with paleomagnetic rotations of rock

units in the opposite sense observed on the east and west sides of the Aegean [e.g., *Kissel and Laj*, 1988]. This earlier episode of deformation was discontinuous both in time and in space [*Mercier et al.*, 1989]. Unlike the present episode of deformation, the North Anatolian fault (initiated and active only since the Pliocene time) was not involved in this earlier deformation.

[5] The nature of the forces responsible for the complex motion of the Aegean is a subject of debate. Deformation may result from forces applied to the edges of rigid blocks [e.g., *Taymaz et al.*, 1991], from forces acting within the mantle [e.g., *Makris*, 1976], from buoyancy forces [e.g., *Le Pichon et al.*, 1982; *Hatzfeld et al.*, 1997], from the sudden slab retreat due to a tear in the subducting slab [*Sorel et al.*, 1988; *Jolivet*, 2001], or some combination of these. Higher-resolution images of the seismic structure to deeper depths than previously available will help resolve these questions.

[6] The lithospheric structure in the Aegean area has been the focus of many studies. Traveltime analysis from local and regional earthquakes [*Panagiotopoulos and Papazachos*, 1985] resulted in a broad-scale averaged picture of the crustal structure. Refraction profiles mapped the shallow structure beneath specific areas in the Aegean [*Makris*, 1973, 1978; *Makris and Stobbe*, 1984; *Delibasis et al.*, 1988; *Bohnhoff et al.*, 2001; *Clément et al.*, 2004], but the few data that do exist are of varying quality. The most homogeneous image of the Aegean lithospheric velocity structure is deduced from tomographic studies at the scale of the Aegean [*Spakman*, 1986; *Spakman et al.*, 1988; *Drakatos and Drakopoulos*, 1991; *Spakman et al.*, 1993; *Papazachos et al.*, 1995; *Papazachos and Nolet*, 1997]. These large-scale teleseismic and regional studies are complemented by more detailed local tomographic studies using traveltime arrivals recorded by local network [*Christodoulou and Hatzfeld*, 1988; *Ligdas et al.*, 1990; *Ligdas and Main*, 1991; *Ligdas and Lees*, 1993]. These studies all assume a layered starting velocity structure divided into blocks of various sizes and compute lateral variation in the velocity structure. Therefore a traveltime delay for a specific block could be due either to a real low relative velocity zone in the block or to a variation in the thickness of the block. For this reason, tomography may not be the most appropriate tool to map the Moho depth over a large area.

[7] Maps of the Moho topography derived from gravity data image the variation of the crustal thickness in the Aegean [*Le Pichon and Angelier*, 1979; *Makris and Stobbe*, 1984; *Tsokas and Hansen*, 1997; *Tiberi et al.*, 2001; *Tirel et al.*, 2004]. However, all these Moho maps suffer severe limitations due to the corrections made for the subducted slab and the thickness of the shallow sediments. As a result, the Moho maps provided by *Tsokas and Hansen* [1997] or *Makris and Stobbe* [1984] and recently by *Tirel et al.* [2004] show considerable differences.

[8] *Karagianni et al.* [2005] used Rayleigh wave group velocities to infer a three-dimensional (3-D) tomographic image of the shear wave velocity structure of the crust and upper mantle in the Aegean Sea using regional events. This work is complemented with a group and phase velocity study at longer period using teleseismic events [*Bourova et al.*, 2005]. They found different crustal thicknesses in the Aegean Sea and beneath Greece, which are in agreement with the general characteristics estimated from previous works in this area.

[9] In general, thicker crust (40–45 km) exists beneath western Greece and the Peloponnesus along the Hellenides mountain range [*Makris*, 1976; *Papazachos and Nolet*, 1997; *Tsokas and Hansen*, 1997; *Tiberi et al.*, 2000; *Karagianni et al.*, 2002, 2005], while thinner crust (30–34 km) is found below eastern Greece. In the southern Aegean Sea, the crust is approximately 20–30 km thick, whereas the northern Aegean Sea exhibits a crustal thickness of about 25–30 km [*Makris*, 1976; *Papazachos and Nolet*, 1997; *Tsokas and Hansen*, 1997; *Tiberi et al.*, 2000; *Knapmeyer and Harjes*, 2000; *Karagianni et al.*, 2002; *Marone et al.*, 2003; *Karagianni et al.*, 2005]. The complexity of the crustal structure beneath the island of Crete, probably due to its location in the forearc of the subduction zone, has been shown in a number of studies [*Makris*, 1978; *Knapmeyer and Harjes*, 2000; *Bohnhoff et al.*, 2001; *Li et al.*, 2003; *Endrun et al.*, 2004], but the average crustal thickness of Crete is about 28–30 km.

[10] The subducted African plate is imaged as a velocity feature at least down to 600 km depth [*Spakman et al.*, 1988; *Wortel et al.*, 1990; *Papazachos and Nolet*, 1997]; however, the zone of seismicity terminates at a depth of about 180 km [*Papazachos and Comninakis*, 1971]. The subducted African lithosphere resolved from seismicity [*Makropoulos and Burton*, 1984; *Papazachos*, 1990; *Hatzfeld and Martin*, 1992; *Papazachos et al.*, 2000] and seismic tomography [*Papazachos et al.*, 1995; *Papazachos and Nolet*, 1997] shows a remarkable shape with an increasing dip from west to the east.

[11] Receiver function studies of the lithospheric structure in the Aegean area and Greece are more limited. The early work of *Knapmeyer and Harjes* [2000] using P receiver functions in western Crete showed a downgoing oceanic Moho at a depth of 40–70 km, while *Li et al.* [2003] mapped the Moho to a depth of 100 km beneath Santorini in the volcanic arc. However, the absence of seismological stations in the Sea of Crete makes this structure difficult to investigate with P receiver functions (Figure 1).

[12] The main goal of this paper is to derive a more homogeneous image of the crustal thickness and subducting African lithosphere for the entire Aegean area from direct seismological observations. To achieve this goal, we employ the P and S receiver function technique to existing data recorded by 65 stations belonging to various seismological networks across continental Greece, the Aegean Sea and the island of Crete. P receiver functions resolve the most prominent structures beneath each seismological station, however, they suffer from multiples. S receiver functions are essentially free of multiples and provide information on structures at greater distances from the seismic stations than do P receiver functions and therefore enhance the spatial sampling of the earth structure.

2. Data and Method of Analysis

2.1. Data

[13] Four different data sets were combined to construct a dense coverage of the Aegean region (Figure 1). The first data set consists of 22 stations from a temporary network operated for six months in 1997 (the Seisfaultgreece project

[*Hatzfeld et al.*, 2001]) using Lennartz LE5S, Güralp CMG40 and Güralp CMG3 seismometers (labeled Sfg in Figure 1). The second data set consists of recordings from 8 permanent broadband stations from the GEOFON (http://www.gfz-potsdam.de/geofon/) network on the island of Crete and in the southern Aegean Sea. These stations are equipped with STS2 seismometers and have been in operation since 1996. To further improve spatial coverage on the island of Crete, we used data recorded from one broadband MEDNET (http://mednet.ingv.it/) station equipped with a STS2 sensor. The third data set consists of recordings from 21 permanent stations of the National Observatory of Athens (NOA; http://www.gein.noa.gr/). These sites have either Lennartz LE20S or Güralp CMG40 seismometers and have been in operation since March 2003. The fourth data set consists of recordings from 22 temporary seismographs (19 Mark L4-3D and 3 STS2 seismometers) of the CYCNET that was operated in 2002–2004 by the Bochum University (http://www.geophysik.ruhr-uni-bochum.de/research/seismology/cyclades/).

2.2. P Receiver Function Technique

[14] The P receiver function method is now a routine seismological technique for constraining crust and upper mantle velocity discontinuities [e.g., *Langston*, 1977; *Owens et al.*, 1984; *Kind and Vinnik*, 1988; *Kosarev et al.*, 1999]. The teleseismic P wave coda contains P-to-S conversions generated at significant and relatively sharp velocity discontinuities in the crust and upper mantle beneath a seismograph site (Figure 2a). The delay time of the converted phase relative to the arrival time of the direct P wave depends on the depth of the discontinuity, the ray parameter of the incident P wave and the velocity of the layers. Rotation of ZNE component waveforms into the local P-SV-SH ray-based coordinate system isolates the Ps converted phases on the SV component, which is perpendicular to the direction of the P component containing the P wave motion. To eliminate the influence of instrument and source parameters, the instrument responses are removed and the P component is deconvolved from the SV component. The final P receiver function contains, in addition to the primary converted phases, multiple phases generated by reflections between the Earth's surface and velocity discontinuities (Figure 2c, first panel).

[15] Positive amplitudes in the P receiver function indicate a velocity increase with depth, whereas negative amplitudes indicate a velocity decrease with depth. Including the multiples in the receiver function analysis gives additional information about the depth of the Moho discontinuity and the Poisson's ratio of the crust [*Zandt and Ammon*, 1995; *Zhu and Kanamori*, 2000; *Yuan et al.*, 2002]. However, the presence of significant sediments may cause large amplitude reverberations masking the primary Ps converted phases and make the estimation of the discontinuity depth difficult.

2.3. S Receiver Function Technique

[16] S-to-P conversions produced at significant velocity discontinuities beneath the station (Figure 2a) can be obtained by deconvolving the SV component from the P component. S receiver functions have a significant advantage over P receiver functions because the converted Sp phase arrives earlier than the main S phase [e.g., *Faber and Müller*, 1980; *Bock*, 1991; *Farra and Vinnik*, 2000; *Li et al.*, 2004; *Kumar et al.*, 2005a, 2005b; *Sodoudi et al.*, 2006], and therefore upper mantle conversions are free from interference of crustal multiples (Figure 2c, second panel).

[17] The converted Sp phases are generally best observed at epicentral distances between 60° and 85° [*Faber and Müller*, 1980]. Since the time difference between converted Sp and S waves depends on the ray parameter, we correct the S-to-P conversions to a common distance using a reference slowness of 6.4 s/deg. Although this velocity is not necessarily realistic for S waves, it is used to make P and S receiver function timescales directly comparable. S receiver functions are much noisier than P receiver functions due to their later arrival times. They also have longer periods in comparison with the P receiver functions and resolve less fine structure within the crust and mantle lithosphere. However, the fact that they are free of multiples enables the identification of Sp conversions at mantle discontinuities. Therefore mantle discontinuity conversions, which are masked by crustal multiples arriving at nearly the same time in P receiver functions, can be isolated in the S receiver functions (Figure 2c).

[18] Figure 2c shows synthetic P and S receiver functions obtained from a simple two-layered model over a half-space (Figure 2b) containing the crust-mantle and the lithosphere-asthenosphere boundaries at 30 and 125 km depth, respectively. The P onset (for P receiver function) and S onset (for S receiver function) are fixed to be at zero time. While a Ps converted phase at the Moho boundary (Figure 2c, first panel) arrives later than the direct P wave, the converted Sp Moho phase is a precursor of the direct S wave, and cannot be disturbed by multiples (Figure 2c, second panel). The computed P receiver function shows the converted Ps phase at the Moho boundary as well as its multiples (Figure 2c, first panel). The converted phase from the lithosphere-asthenophere boundary (labeled LAB) is in this case masked by the Moho multiple (with negative amplitude) arriving at the same time in the P receiver function. This boundary is however clearly observed in the S receiver function at ~14 s reversed time (Figure 2c, second panel). To make the S receiver functions directly comparable with the P receiver functions, we reverse the time axis (Figure 2c, third panel) and the polarities of the S receiver functions (Figure 2c, fourth panel; see also *Yuan et al.* [2006]). Therefore, consistent with the P receiver function, positive amplitude in the S receiver function indicates an increasing velocity with depth.

3. Observations

3.1. P Receiver Functions

[19] To compute P receiver functions, we select teleseismic records for events with magnitude greater than m_b 5.5 and epicentral distances ranging between 30° and 95°. Receiver functions filtered between 1 and 20 s and corrected to a reference distance of 67° are shown for two stations, LIMN and NEO in Figure 3 (see Figure 1 for stations location). At LIMN, the primary converted phase from the continental Aegean Moho and its first multiple arrive at a delay time of approximately 3.4 s and 10 s, respectively, while those at NEO are observed at approximately 3.3 s and

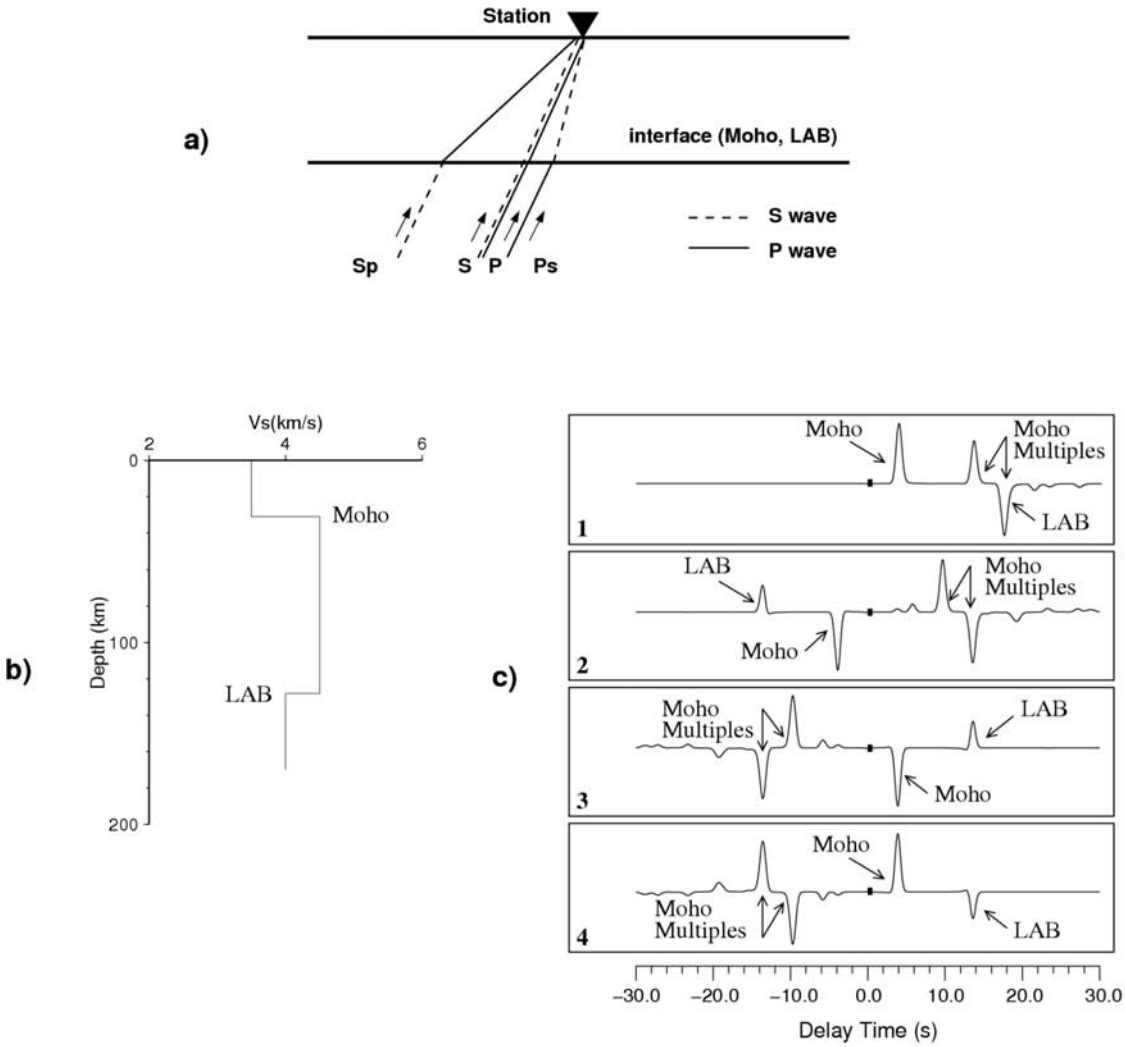

Figure 2. (a) Raypaths of P and S receiver functions. (b) A two-layered model over a half-space consisting of two discontinuities: the crust-mantle boundary at 30 km and the lithosphere-asthenophere boundary at 125 km. The S velocity is considered to be 3.5 km/s in the crust and 4.5 km/s in the upper most mantle. (c) Synthetic P and S receiver functions computed for the model shown in Figure 2b. The P onset for P receiver function and the S onset for S receiver function are fixed at zero time (bold thick line). In the first panel, the P receiver function significantly reveals the Ps conversion at the Moho and its multiple phases, while the lithosphere-asthenosphere boundary (labeled with LAB) is masked by the crustal multiple with negative amplitude. In the second panel, in contrast, the S receiver function reliably shows the Sp converted phase from the Moho as well as that from the LAB. Sp phases arrive earlier than direct S waves, whereas all the multiples appear later. The polarity of the Sp converted phase is reversed due to the different sign of its conversion coefficient comparing to that of Ps. In the third panel, to make it directly comparable with the P receiver function, the time axis is reversed, and in the fourth panel, polarities of the Sp phases are also reversed.

11 s, respectively. Some energy is observed at the zero time at station NEO suggesting that either the rotation of the components is not optimal or shallow sediments generate some energy.

[20] We compute P receiver functions for all stations and summarize the results in the stacked moveout-corrected receiver functions shown in Figure 4. These traces are sorted by their south-to-north distance from the Hellenic trench, and provide an average discontinuity depth beneath each station. The P receiver functions are plotted in a time window of 0–20 s in order to display information for both continental and oceanic structures.

[21] The receiver functions obtained for stations in the southern Aegean and on the island of Crete (labeled FA in Figure 4) show a phase with increasing delay time northward, reaching 10 s beneath the volcanic arc. This phase is interpreted as the Moho of the subducted African plate (labeled African Moho). It can be followed from 4.5 s beneath station VLS to 11 s beneath station SANT in the volcanic arc (labeled VA in Figure 4). North of SANT, this phase is no longer clear. Beneath the northern Aegean Sea

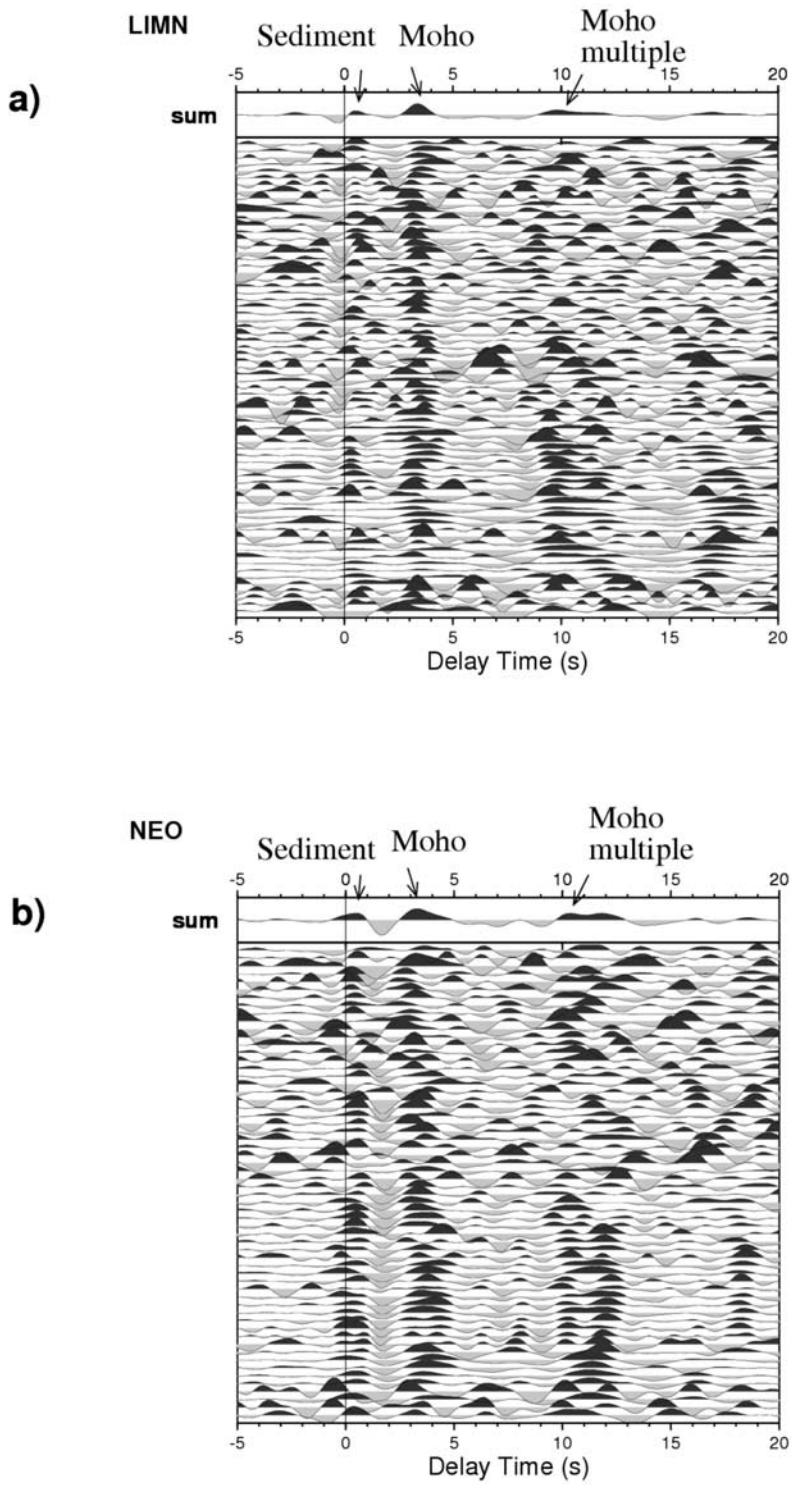

Figure 3. (a) Individual P receiver functions for station LIMN located in the northern Aegean Sea. Positive amplitudes are plotted in black, and negative amplitudes are shown in gray. Individual seismograms are plotted equally spaced and sorted according to their back azimuth. The Ps conversion phase from the Aegean Moho and its multiple and the Ps conversion from the sediment layer are labeled on the summation trace. (b) Same for station NEO located in mainland Greece.

and continental Greece (labeled NA and CG in Figure 4, respectively), the strongest phase observed between 3 and 4.8 s (labeled Aegean Moho) is interpreted to be the Ps conversion from the Moho of the continental Aegean plate. This phase is not well observed under the forearc (FA in Figure 4). There it is replaced by a significant negative

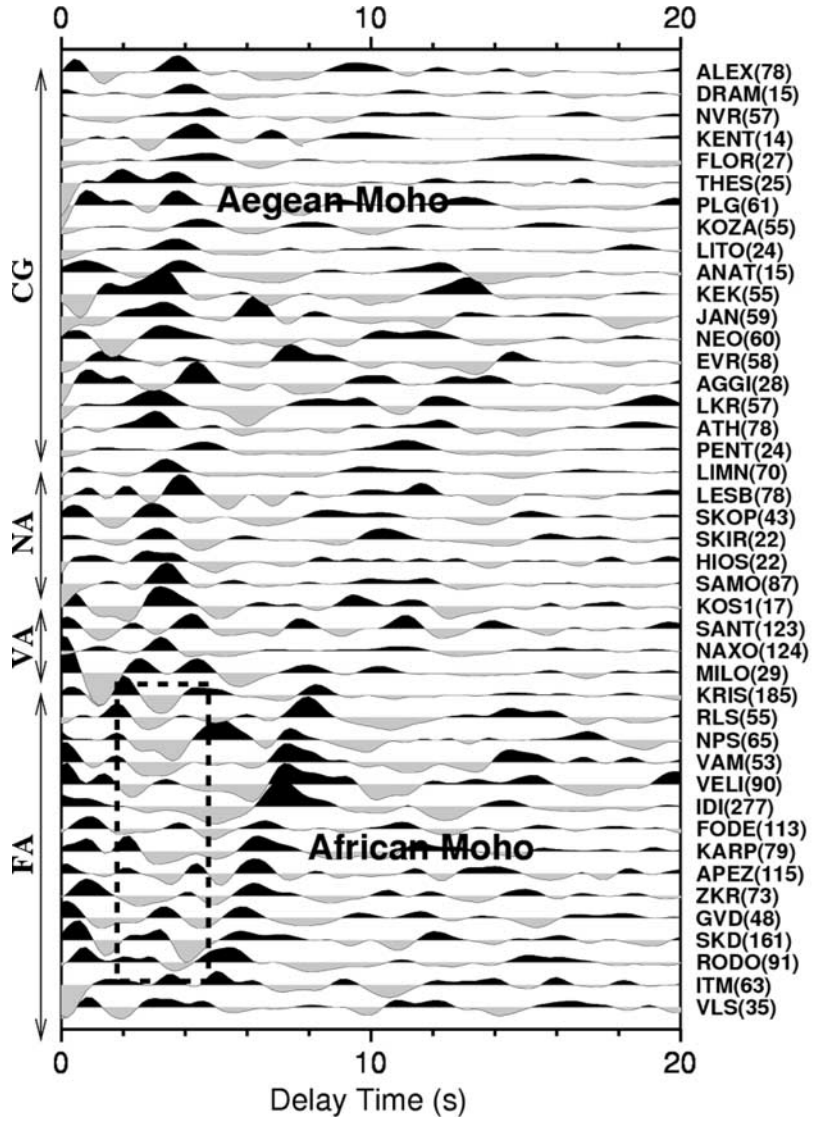

Figure 4. Stacked P receiver functions sorted according to their distance from the Hellenic trench from south to north. The north dipping phase in the southern part labeled "African Moho" indicates Ps conversions from the Moho of the subducting African lithosphere. This phase can be traced from station VLS to the station SANT in the volcanic arc. Ps conversions from the Moho of the continental Aegean lithosphere (labeled Aegean Moho) are observed in the northern part and disappear southward. The black dashed box indicates negative conversions which are seen at the expected Moho conversion times. The number of P receiver functions for each station is shown in brackets. FA, forearc; VA, volcanic arc; NA, northern Aegean; CG, continental Greece.

amplitude phase (dashed box in Figure 4). This negative phase was also reported for most stations located on Crete [*Knapmeyer and Harjes*, 2000; *Li et al.*, 2003; *Endrun et al.*, 2004].

[22] In Figure 5, the stacked receiver functions are sorted by increasing time of the converted Ps phase from the Aegean Moho. Stations from the forearc with possibly negative Moho signals are not contained in Figure 5. The data show clear primary Moho conversions where the amplitude of the Moho multiples appear to be reduced since we used the moveout curve for direct Ps conversions and not that for multiples. To compute the depth of the Aegean Moho beneath the stations, we used an average crustal velocity of 6.2 km/s and a Vp/Vs ratio of 1.73. This is a first-order estimate of the Aegean velocity structure and keeps our depth values independent from possible errors of preliminary shear velocity models. However, we estimate the deviation to this model to be less than 5%. Therefore this procedure results in an 1.5–2 km error in the Moho depth determination. The calculated Aegean Moho depths are listed in Table 1. We could not estimate the delay times of the converted phases from the Aegean Moho at stations in the forearc region due to the presence of unclear negative signals.

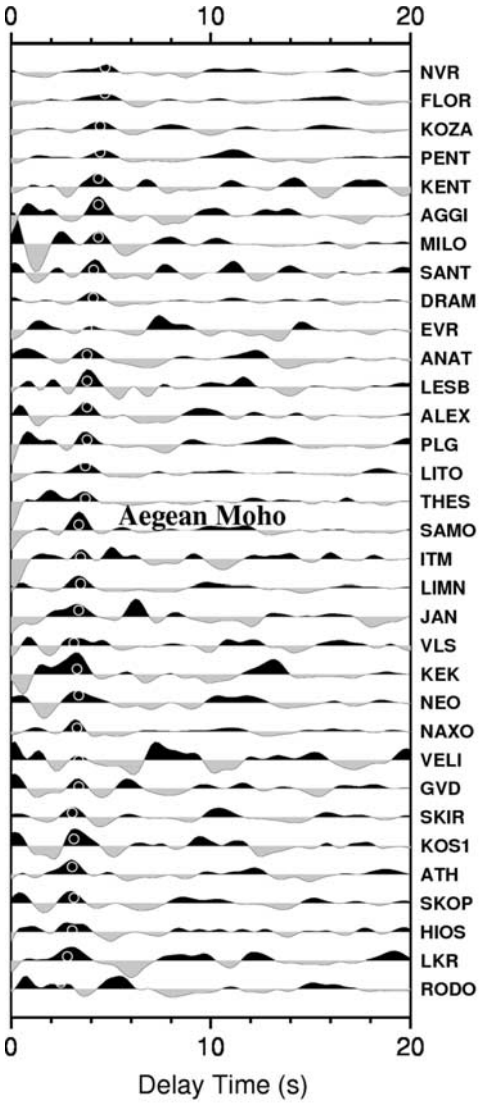

Figure 5. Estimated arrival times of Moho conversions (Aegean Moho), displayed with white circles for stations with positive amplitudes and sorted according to their values from 3 to 4.8 s. The stacked receiver functions are filtered with 1–20 s band-pass filter. Arrival times are converted to depth (km) using a Vp of 6.2 and a Vp/Vs ratio of 1.73. Moho conversion times and depths are listed in Table 1.

3.2. S Receiver Functions

[23] We compute S receiver functions from seismograms of events with magnitude greater than 5.7 (mb) and epicentral distances between 60° and 85° for 50 of the stations within the area. Moveout corrected and band-pass-filtered (6–20 s) S receiver functions at the GEOFON station KRIS located on the island of Crete are shown in Figure 6. The first phase at about 3 s (labeled Aegean Moho) represents the converted Sp phase from the Aegean Moho discontinuity; the second phase at about 8 s (labeled African Moho) is associated with the Moho of the subducted African lithosphere; and the third phase with a strong negative amplitude at about 13 s delay time (labeled LAB) is interpreted as a conversion from the lithosphere-asthenosphere boundary.

[24] Figure 7 shows the location of the Ps and Sp piercing points at 80 km depth. This depth was chosen based on the P receiver functions, which show the African Moho at delay times ranging from 8 to 10 s beneath the southern Aegean Sea (see also Figure 4). As Figure 7 shows, while P piercing points are located close to the stations, S piercing points are located much farther away from the stations. Therefore the two together provide reasonably dense spatial coverage (see also Figure 2a). For example, while the Sea of Crete is poorly sampled by the P receiver function observations, it is well covered by S receiver function observations. We plot two sets of cross sections from S receiver functions (Figure 8). The first set consists of three parallel S-N trending cross sections across the Aegean and continental Greece (Figures 8a–8c).

Table 1. Stations, Geographical Coordinates, Ps Conversion Times at the Aegean Moho and Their Corresponding Depths, Ps Conversion Times at the African Moho, and Their Corresponding Depths

			Aegean Moho		African Moho	
Stations	Longitude	Latitude	Time, s	Depth, km	Time, s	Depth, km
AGGI	22.32	39.01	4.4	36	-	-
ALEX	25.79	40.97	3.7	30	-	-
ANAT	22.68	39.74	3.8	31	-	-
APEZ[a]	24.88	34.97	4	33	6.2	52
ATH	23.72	37.97	3.1	25.5	-	-
DRAM	24.01	41.2	4.1	34	-	-
EVR	21.81	38.92	4	33	-	-
FODE[a]	24.95	35.37	4	33	6.7	58
FLOR	21.38	40.78	4.8	40	-	-
GVD	24.08	34.83	3.3	27	5.8	48.5
HIOS	26.04	38.25	3	25	-	-
IDI[a]	24.89	35.28	4	33	7.1	61
ITM	21.93	37.18	3.5	28.5	5	41
JAN	20.85	39.66	3.4	28	-	-
KARP	27.17	35.55	-	-	6.2	52
KEK	19.8	39.71	3.3	27	-	-
KOS1	27.21	36.84	3.2	26	-	-
KOZA	21.78	40.3	4.5	37	-	-
KRIS[a]	25.5	35.17	2.5	21	8.1	70
LESB	26.26	39.24	3.8	31	-	-
LIMN	25.16	39.95	3.4	28	-	-
LITO	22.48	40.1	3.7	30	-	-
LKR	23	38.65	3	25	-	-
MILO	24.44	36.67	4.4	36	10.2	90.5
NAXO	25.52	37.07	3.3	27	-	-
NEO	23.22	39.31	3.3	27	-	-
NPS[a]	25.61	35.26	2.5	21	7.4	64
NVR	23.86	41.35	4.8	40	-	-
PENT	23.96	38.04	4.5	37	-	-
PLG	23.45	40.37	3.7	30	-	-
RLS[a]	21.47	38.06	3	25	8	69.5
RODO	28.02	36.08	3	25	5.5	46
SAMO	26.83	37.7	3.5	28.5	-	-
SANT	25.45	36.37	4.2	34.5	11.1	99
SKD[a]	23.92	35.41	4	33	7.2	62
SKIR	24.57	38.85	3.2	26	-	-
SKOP	23.74	39.11	3	25	-	-
THES	22.96	40.63	3.6	29.5	-	100
VAM[a]	24.2	35.41	4	33	7.3	63
VELI	22.94	36.71	3.3	27	7.2	62
VLS	20.59	38.18	3.4	28	4.5	36.5
ZKR[a]	26.31	35.11	3.1	25.5	6.2	52

[a]No observed positive Ps Moho conversion, the delay times of Moho conversions are inferred from S receiver functions.

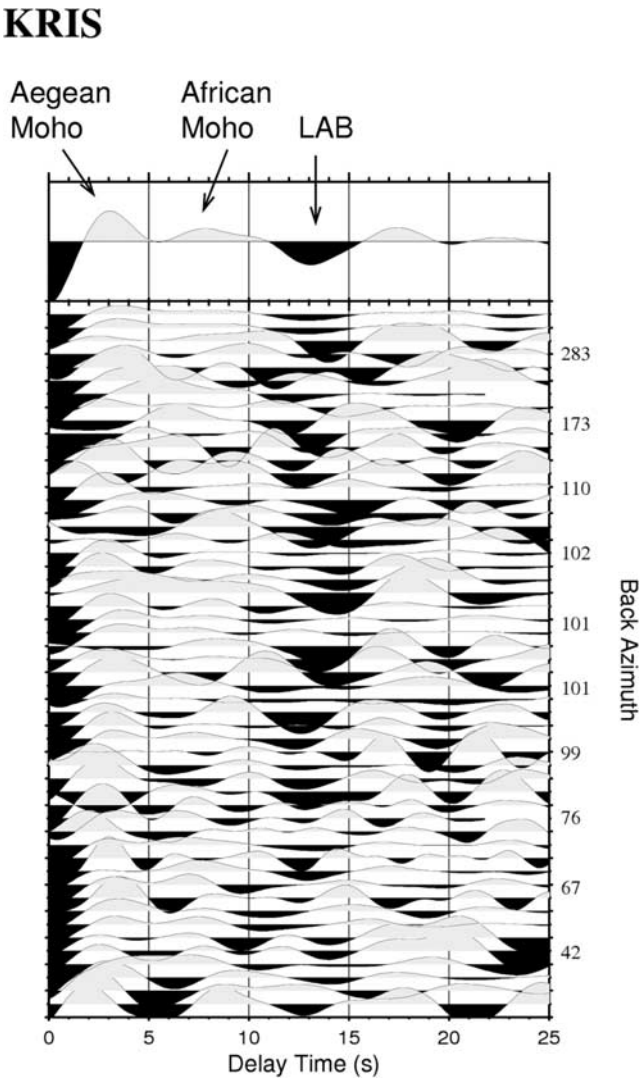

Figure 6. The 53 individual S receiver functions for broadband station KRIS on Crete sorted by back azimuth. The S receiver functions are plotted in reversed time and reversed polarities to allow direct comparison with P receiver functions. The arrows on the stacked trace (top) show the average time of the Sp conversions generated by the continental Aegean Moho, the oceanic Moho of the subducted African plate and the lithosphere-asthenosphere boundary, respectively.

The second set consists of three profiles perpendicular to the Hellenic trench (Figures 8d–8f). Individual S receiver functions are considered in the data bands of 1.25° at each side of the profiles and sorted by the latitude of their piercing points at 80 km depth. A 4 s low-pass filter is applied to the data. Although they are much noisier than stacked data, they allow a more detailed image of the geometry of the Aegean Moho and of the subducting slab. The traces in Figure 8 are plotted in trace spacing. That means all traces are equally spaced in the sequence of their latitude, but not in a linear scale. This is a good technique for screening all individual traces and for detecting phases correlatable over larger distances. In order to obtain sections with a linear latitude-scale, traces must be binned. We divide the region into 39 boxes (see also Figure 7) and a stacked S receiver function is computed for each box from all individual S receiver functions (Figure 8) whose piercing point (at 80 km) fell into the respective box. It is important to note that the 80 km deep piercing point is not appropriate for deeper phases with later arrival times (~15–20 s). Therefore, for the northern Aegean and mainland Greece, the data are also sorted with piercing points at 200 km depth in the same boxes. However, no considerable difference is observed in the arrival times of the seismic phases beneath the northern part of the area if we use piercing points at 200 km depth. In Figure 9, stacked S receiver functions computed for each box (see Figure 7) are shown along profiles DD^1-FF^1 (see Figures 8d–8f). The stacking method enhances the conversions and reduces the error of the depth determination by averaging the information of many single traces within each box. Note that the African Moho obtained by stacked data in Figure 9 is similar to that obtained from individual traces in Figures 8d–8f.

3.3. Moho Topography of the Subducting African Plate

[25] Figure 10 shows a map of the topography of the African Moho derived from our data. This map combines results from P and S receiver function techniques. Along the Hellenic arc, results from stacked P receiver functions from 17 stations are used (data from Figure 4). The 17 station locations are indicated by triangles in Figure 10. At larger depths, where P receiver functions poorly resolve the African Moho, stacked S receiver functions in the boxes of Figure 7 are used to determine the times of the Moho conversions (Figures 8 and 9). The centers of the boxes are also marked in Figure 10 (white small points). Depths are determined from delay times using the IASP91 reference model [*Kennett and Engdahl*, 1991]. Because of the absence of a model covering the entire area, we preferred to use a well known and frequently used global reference model for the depth determination. The times and depths of the African Moho at stations and boxes are given in Tables 1 and 2, respectively. The delay times in Tables 1 and 2 may be used later with improved P and S velocity models to infer depths. Future improved receiver function observations might, for example, be able to resolve multiples, which would be very helpful for determining Vp/Vs ratios [*Zhu and Kanamori*, 2000]. In the following, we describe the African Moho imaged by cross sections AA^1-FF^1 (Figure 8).

[26] In addition to the Sp conversion at the Aegean Moho, which can be seen between 2.5 and 4 s along profile AA^1 (Figure 8a), we clearly observe the Moho of the subducting African plate (labeled African Moho). This phase can be traced from 6 s (~50 km deep) in the southern Aegean to about 25 s (~220 km deep) in northern Greece. Because of the lack of seismological stations in the Aegean Sea this phase could only be imaged by P receiver functions to 10 s beneath station SANT in the volcanic arc (see also Figure 4). The subducted African lithosphere has been imaged by tomography down to 600 km [*Spakman et al.*, 1988] and even to 1200 km [*Bijwaard et al.*, 1998] beneath northern Greece. *Papazachos et al.* [1995] also reported the continuity of the African lithosphere up to northern Greece by tomographic images, even though the deepest earth-

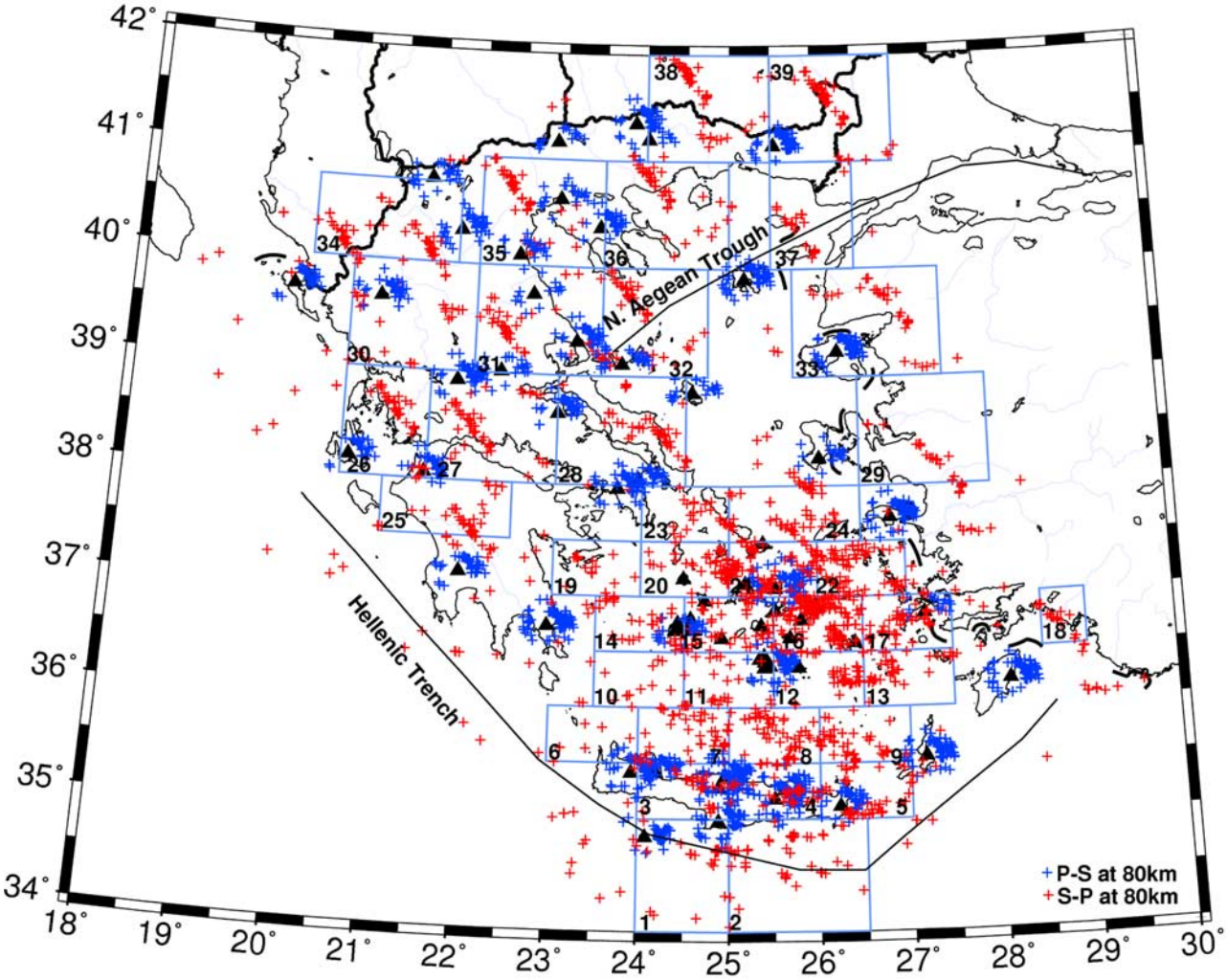

Figure 7. Location of piercing points of P (blue crosses) and S (red crosses) receiver functions at 80 km depth. Triangles denote stations. Because of the differing ray parameters for Ps and Sp conversions, the Cretan Sea is well covered with S piercing points and so compliment the P receiver functions. The study area is divided into 39 boxes that sample different geological formations relative to the positions of S piercing points.

quakes are at depths of approximately 180 km in the eastern part of the trench (see also Figure 1).

[27] Along profile AA[1], the African Moho has a noticeably variable downgoing slope. It starts at low angle (~10°) in the southern Aegean and becomes steeper under the volcanic arc (~30°). It flattens out beneath the central Aegean and then steepens again beneath northern Aegean Sea and continental Greece. In the central part of the Hellenic subduction zone (along profile BB[1]), the African Moho is clearly deeper than in the eastern part. It can be followed from 9 s in the southern Aegean to 23 s beneath northern Greece. It also dips gradually at a low angle (~10°) to the northern Aegean and becomes horizontal toward mainland Greece. Beneath the western Peloponnesus and western Greece (profile CC[1]), the African Moho is shallow (delay time 5–6 s) and the arrival time of this converted phase is very close to that of the Aegean Moho converted phase. The phase at 5–6 s has generally been interpreted as related to the Aegean Moho boundary at 45 km depth [e.g., *Karagianni et al.*, 2002; *van der Meijde et al.*, 2003; *Karagianni et al.*, 2005]. However, Figure 8c indicates that the converted phase at 5 s beneath the Peloponnesus is associated with the African Moho. The African Moho is almost horizontal beneath the Peloponnesus, dips steeply (~45°) beneath the Gulf of Corinth and flattens out under continental Greece. This result is also consistent with the shallow seismicity recorded beneath the Peloponnesus [*Hatzfeld*, 1989; *Papazachos et al.*, 2000].

[28] It is interesting to note that all three S receiver function profiles in Figures 8d–8f demonstrate a significant Moho phase with positive amplitude in the forearc area, while P receiver functions exhibit a reversed Moho velocity contrast (see also Figure 4). Profile DD[1] indicates a steeper African Moho in the eastern part in comparison with other parts of the arc. The continuity of the subducted plate up to northern Greece is well illustrated in profile EE[1]. The African Moho is also visible to about 25 s (~220 km) along this profile. *Spakman et al.* [1988] showed the

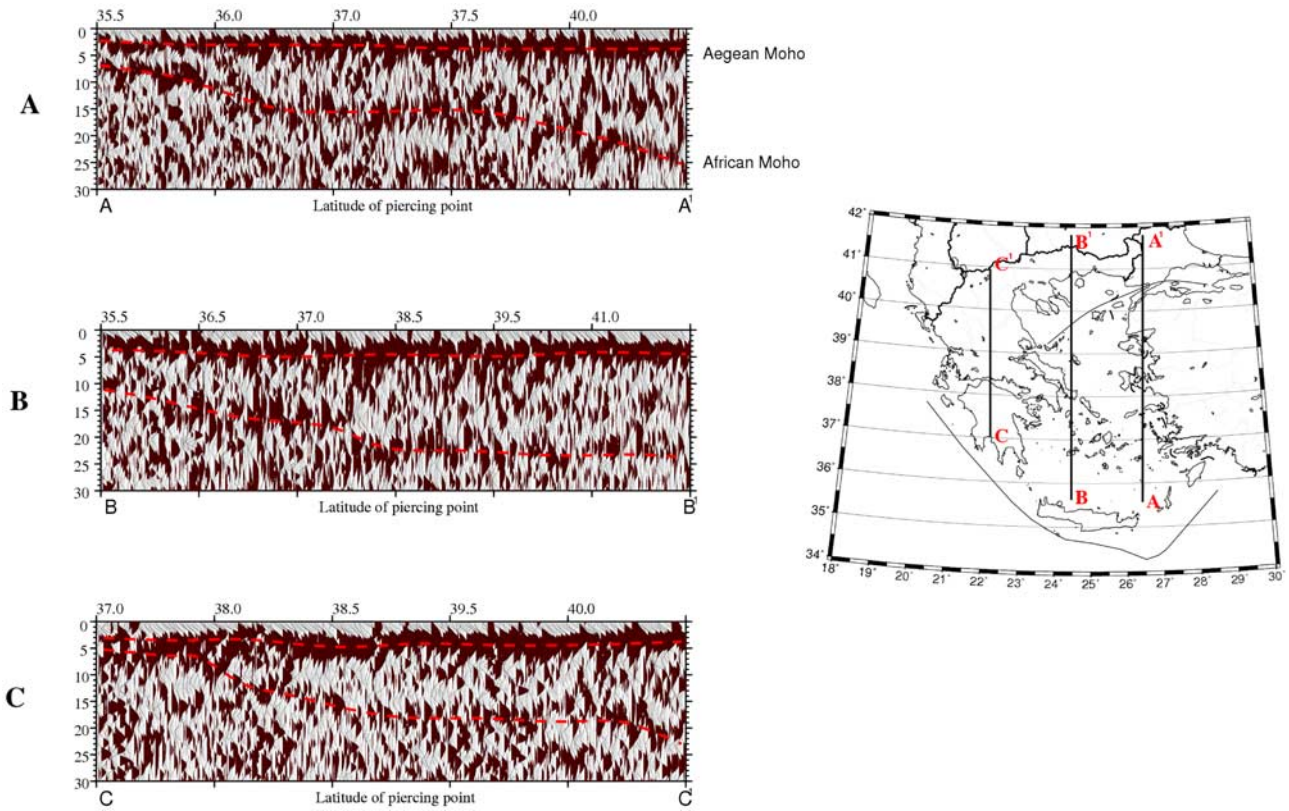

Figure 8. Imaged structures deduced from individual S receiver functions along S-N trending profiles AA^1-CC^1 and profiles DD^1-FF^1 orientated perpendicular to the trench. The individual S receiver functions are considered in the data bands of 1.25° at each side of the profiles and sorted by the latitude of their piercing points at 80 km depth (see also Figure 7). They are filtered with a low-pass filter of 4 s. The converted phases are denoted by red dashed lines. The first arriving converted phase (labeled Aegean Moho) is related to the continental Aegean Moho and the second to the subducting African Moho (labeled African Moho). (a) Individual S receiver functions sorted by latitude of S piercing points at 80 km along profile AA^1. The Aegean Moho and the downgoing African Moho are well imaged up to northern Greece. (b) Same for profile BB^1 located in the middle part of the Hellenic arc. (c) Same for profile CC^1 located in the Peloponnesus, west of the Hellenic arc. The downgoing African Moho is reliably observed at ~5 s delay time under the Peloponnesus. (d) Individual S receiver functions along profile DD^1 in the eastern part of the Hellenic arc. (e) Same for profile EE^1 in the middle part of the arc, which crosses the central Crete. (f) Same for profile FF^1 in the western part of the Hellenic arc. The subducting African Moho is well imaged up to continental Greece. The southern part of the African Moho along profile FF^1 is imaged shallower than along profiles DD^1 and EE^1.

existence of a subduction zone at a depth of about 600 km under northern Greece along a similar profile. This might imply that receiver functions can only image the shallow dipping part of the slab down to 200 km in this region. The slab depth along profile FF^1 is consistent with that from profile CC^1. It shows a subhorizontal African Moho beneath the Peloponnesus but increasing dip in the northern Aegean Sea to a depth of about 220 km. A difference in slope reported by the seismicity [*Hatzfeld*, 1989] and tomographic images [*Papazachos and Nolet*, 1997] beneath the Peloponnesus, and interpreted as a kink in the slab at a depth of about 75–95 km, can also be clearly seen in our cross section. Therefore the receiver functions confirm a very shallow dipping slab (slope less than 10°) as far as northern Greece that was mapped by *Papazachos and Nolet* [1997] and, at shallower depth, proposed by *Spakman et al.* [1993].

[29] The observed change in the slope of the African Moho agrees with other geophysical observations. Tomographic results for this region [*Papazachos and Nolet*, 1997] confirm the change in dip of the Moho for different parts of the subducted African plate. *Hatzfeld and Martin* [1992], *Hatzfeld et al.* [1993], and *Papazachos et al.* [2000] imaged the Wadati-Benioff zone in this area and showed that it dips at a shallower angle in the west compared to the east.

[30] On the basis of our results shown in Figure 10, the slope of the African Moho changes laterally. Beneath the Peloponnesus it is almost flat then steepens below the Gulf of Corinth. Further east the African Moho has a moderate dip from Crete to the north of the volcanic arc, but is almost flat beneath the north central Aegean and northernmost Greece. Observed steeper slope of the African Moho

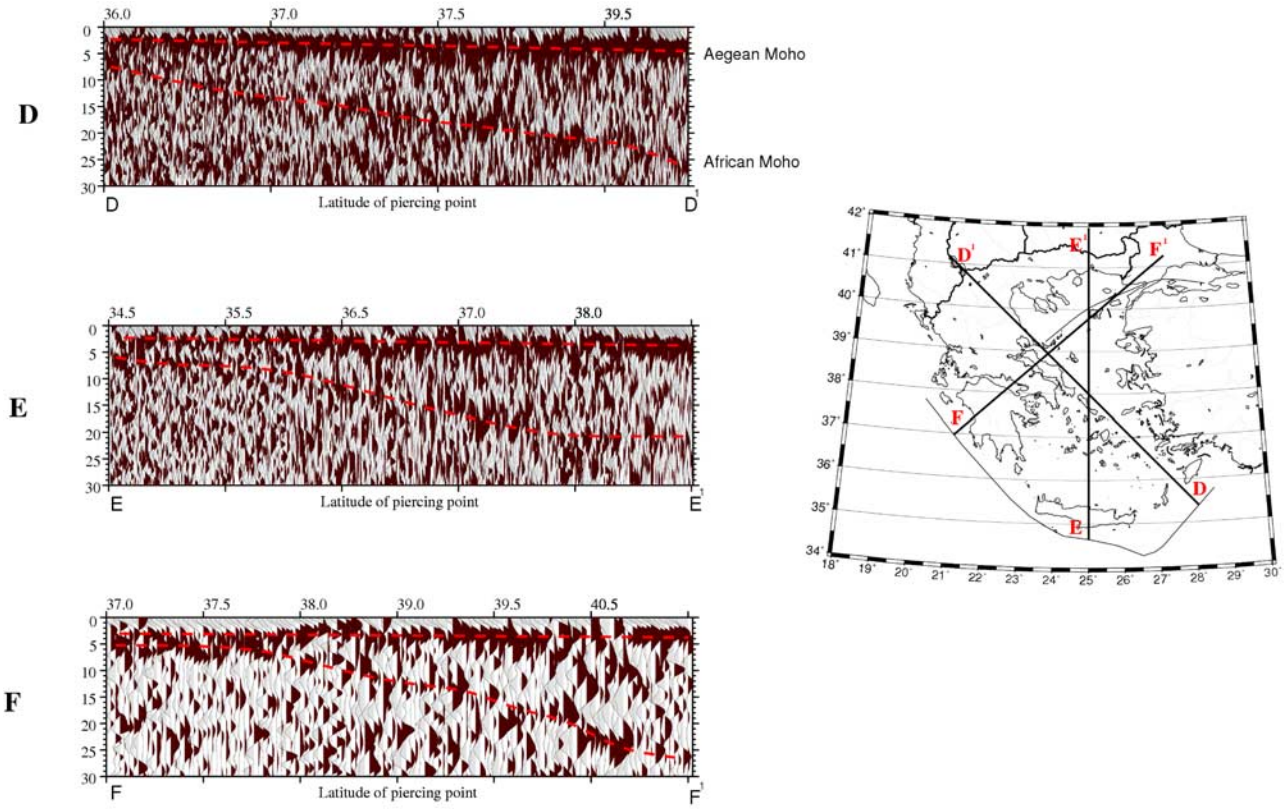

Figure 8. (continued)

beneath the eastern part of the arc where the deepest earthquakes are located (see Figure 1) suggests a faster sinking of the African plate beneath the eastern part rather than the western part of the arc. This is consistent with GPS measurements showing a trenchward motion of 10 mm/yr in the southeastern part of the Aegean relative to the southern Aegean [*McClusky et al.*, 2000].

[31] The depth of the slab (Figure 10) is shallowest (~40–60 km) under the western Peloponnesus, southern Crete and southeast of Rhodes, but its depth increases to 160 km under the volcanic arc. Beneath the northern Aegean and northern Greece, it is continuous and roughly horizontal at a depth of 200–220 km. Tomographic results [*Spakman et al.*, 1988, 1993; *Papazachos et al.*, 1995] show that the subducting slab must extend as far north as the northern Greek border. Therefore it seems that the northern part of the slab is aseismic. *Wortel* [1982] and *Hatzfeld* [1994] demonstrated that reheating of a downgoing slab can affect its rheological properties and limit, if not suppress seismicity.

[32] Hypocenter isodepths of 20, 100, and 170 km in the Hellenic arc provided by *Papazachos et al.* [2000] using data from several temporary networks in the southern Aegean are also denoted in Figure 10. Taking the errors introduced by longer period S receiver functions as well as velocity model (~5–10 km) into account, the earthquake depths are in good agreement with the Moho depths. Furthermore, the African Moho seems to be continuous and flat beneath the northern part of the region suggesting that the subduction was more linear when it started. This supports the idea that the trench has migrated from the northern Aegean to its present position since Eocene [*De Jonge et al.*, 1993]. In addition, the clear continuation of the African Moho from west to east down to a depth of 200 km in our data rules out a possible vertical tear in the slab beneath the Aegean as suggested by *Sorel et al.* [1988].

3.4. Lithosphere-Asthenosphere Boundary of the Aegean and African Plates

[33] Understanding the lithospheric structure is a prerequisite for deciphering the plate tectonics history and the mode of thinning in the Aegean region. Here we provide, for the first time, an image of the lithosphere-asthenosphere boundary (LAB) beneath the Aegean using S receiver functions. In Figure 9 a clear negative phase (shown in black) at ~12–25 s is identified as a conversion from the lithosphere-asthenosphere boundary. The negative phase at delay time ~17 s along the northern parts of profiles DD^1 (box 24-35), EE^1 (box 23-39) and FF^1 (box 28-39) is the LAB of the continental Aegean plate (labeled Aegean LAB in Figure 9). The negative phase at delay time 12 s at the southern end of profiles DD^1 and EE^1, which become increasingly delayed to ~23 s in the central parts of profiles DD^1 and EE^1, is the LAB of the subducting African plate (labeled African LAB). However, this phase arrives at nearly the same time as the Aegean LAB phase along profile FF^1. We converted the delay times of this negative phase to depth using the IASP91 reference model and plotted these depths in Figure 11. Delay times and depth values of the African and Aegean LAB are given in Table 2. Beneath the island and Sea of Crete the LAB is at ~100 km depth but deepens to ~225 km beneath the central Aegean.

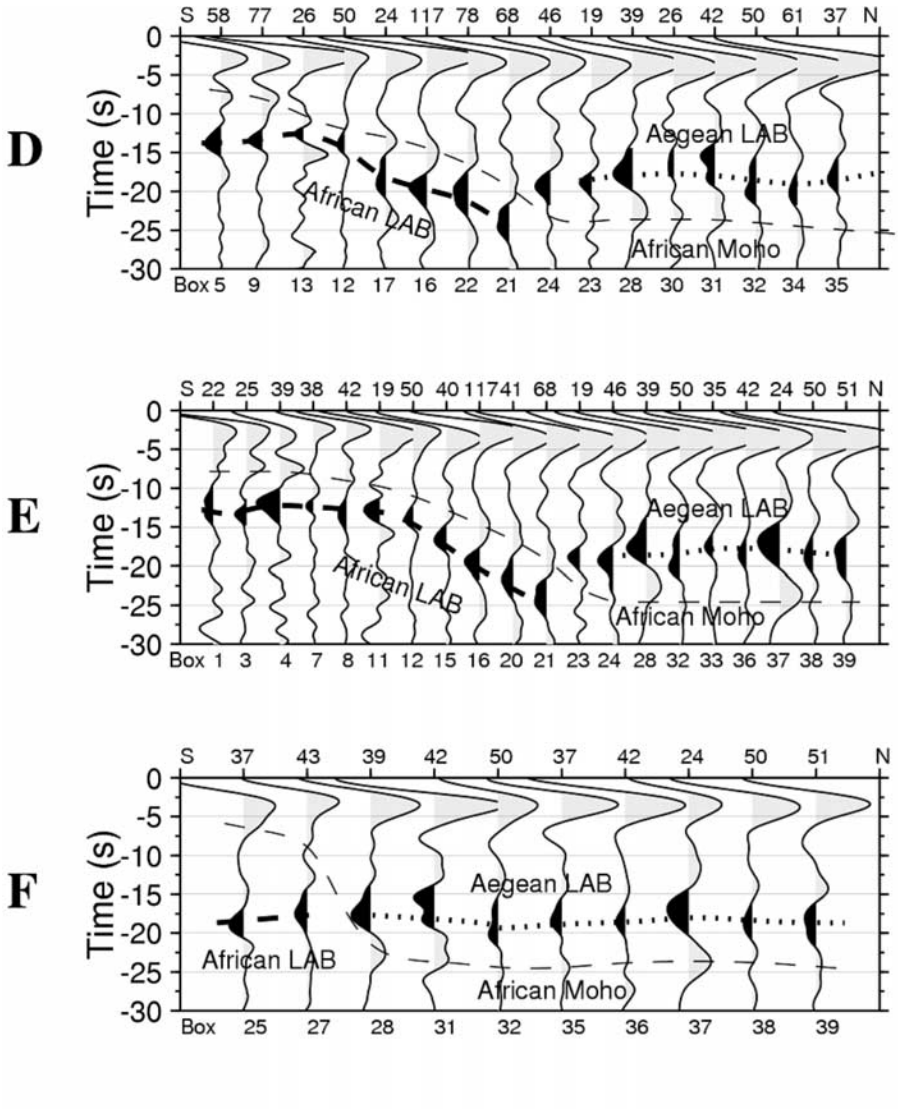

Figure 9. Location of the boundaries estimated from stacked S receiver functions, box by box, along profiles DD^1-FF^1 (Figures 8d–8f). The box number and number of S receiver functions for each box are indicated below and above each trace, respectively. Negative amplitudes of S receiver functions (in black) show a velocity decrease with depth. Different types of lines are used to indicate the African Moho (thin dashed), continental (dotted) and oceanic (thick dashed) LAB. (top) Stacked S receiver functions along profile DD^1 located in the eastern part of the Hellenic arc showing a clear negative phase interpreted as the LAB. The continuation of this boundary is poorly imaged beneath the northern Aegean, due to the absence of piercing points (see Figure 7). Under continental Greece, this negative phase is interpreted as the continental Aegean LAB, which occurs at a shallower depth. The African Moho phases observed in Figure 8 are shown by the thin dashed line and follow the deepening of the African LAB. (middle) Same as Figure 9 (top) but along profile EE^1 in the middle part of the Hellenic arc. Both profiles DD^1 and EE^1 show the continental Aegean LAB at ~17 s, while the oceanic African LAB is dipping from 12 s to 25 s. (bottom) Same as Figure 9 (top) but along profile FF^1 in mainland Greece. Note that the African LAB is at 17 s.

Further north, beneath Greece, the LAB is about 150 km. We interpret the deepening of the LAB from ~100 km in the southern Aegean to ~225 km in the central Aegean as the subduction of the oceanic African lithosphere beneath the Aegean plate. We also interpret the strong horizontal negative phase at about 17 s (at about 150 km depth) above the African Moho phase in mainland Greece as an S-to-P conversion from the continental Aegean lithosphere (Eurasian lithosphere).

[34] Thus it seems that the African lithosphere is thinner than the Aegean (Eurasian) lithosphere (150 km) where we have information. However, we do not have detailed information on the thickness of the Aegean lithosphere beneath the Sea of Crete, which experienced the most important primary stretching. Concerning the Eurasian lithosphere, there

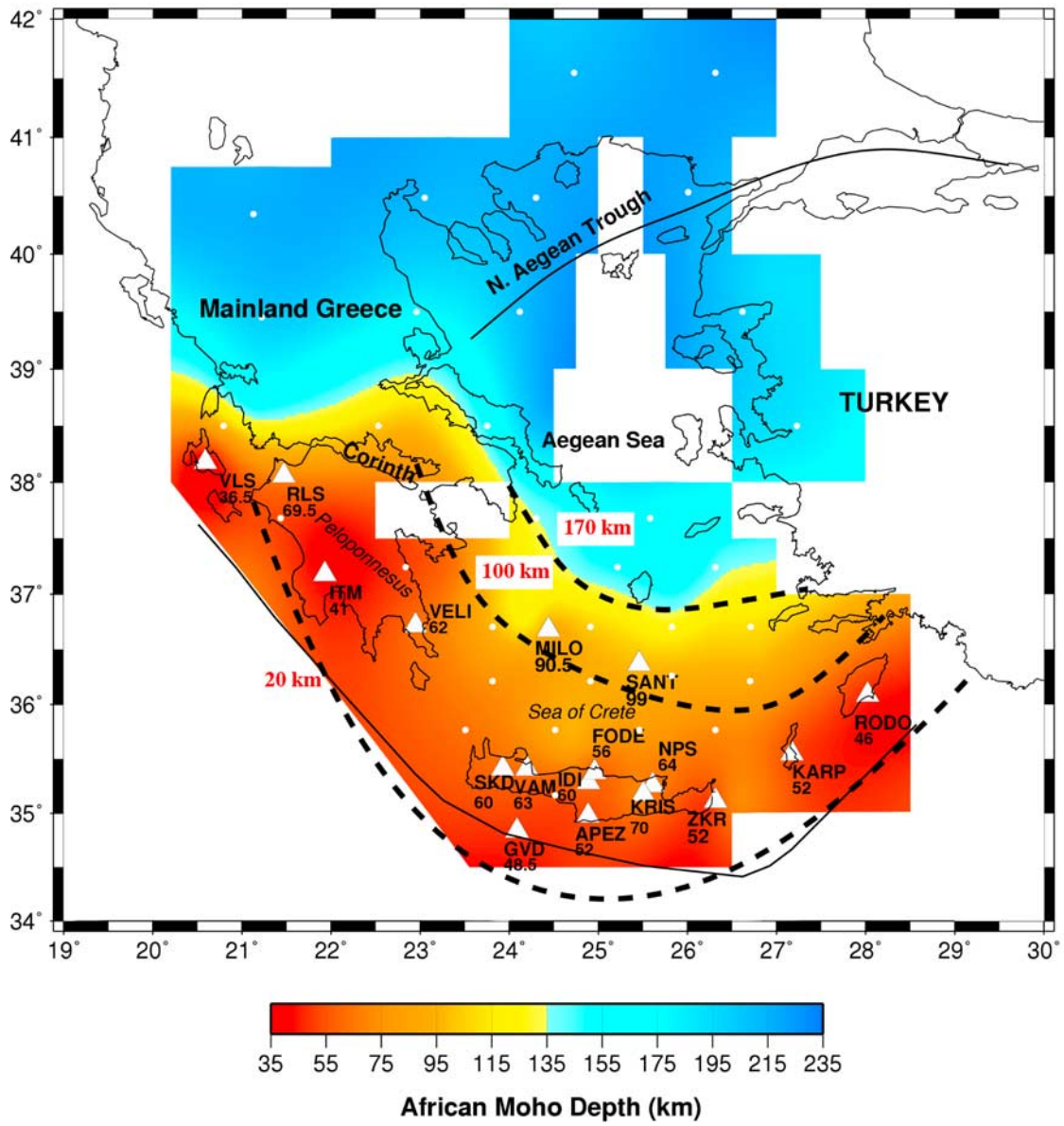

Figure 10. Depth of the African Moho obtained from both P and S receiver functions. Depth values beneath stations represented by triangles are computed using P receiver functions (see also Figure 4). Depth values for other parts of the area are obtained from stacked S receiver functions, box by box (see also Figures 7 and 9). Centers of boxes are shown with small white points. White boxes indicate areas where not enough S piercing points are available. Dashed lines indicate hypocenter isodepths shown for 20, 100, and 170 km and are taken from *Papazachos et al.* [2000].

is no large variation in thickness from continental Greece to the northern Aegean Sea in spite of the large metamorphic core complexes presented in the northern Aegean Sea.

[35] The difference in LAB depth is therefore consistent with a localized stretching process, affecting mostly the southern area of the Aegean, and significantly differs from the present-day stretching rate, which is highest in the northern Aegean Sea. Furthermore, the LAB depth map implies that the lithosphere may not significantly have been involved in the stretching process. The average thickness of the lithosphere in the Mediterranean has been estimated to be 90 km for the Eurasian plate [*Papazachos*, 1969; *Payo*, 1967, 1969], although *Calcagnile et al.* [1982] showed that the Eurasian lithosphere-asthenosphere boundary undulates between 90 and 120 km. According to the error introduced by the selected reference velocity model (~10 km), our results are consistent with those of other studies in this area. Our observations also imply a thickness of 60–65 km for the subducted African lithosphere underneath the Aegean region.

3.5. Aegean Crust

3.5.1. Does a Reversed Moho Contrast Exist in the Forearc?

[36] The S receiver function sections (Figures 8 and 9) show a normal Aegean Moho contrast (i.e., positive ampli-

Table 2. Box Number, Coordinate of the Box Center, Measured Delay Times of Sp Conversions From the African Moho and the LAB as Well as Their Calculated Depths

			African Moho		LAB	
Box	Longitude	Latitude	Time, s	Depth, km	Time, s	Depth, km
1	24.8	34.7	6	50.5	12.5	112.5
2	25.15	34.7	6	50.5	11.3	102
3	24.7	35.3	7	60	13.5	121.5
4	25.7	35.25	7.5	64.5	12	108
5	26.5	35	8	69.5	14	126
7	24.75	35.75	10.5	93	12.4	112
8	25.5	35.75	9	79	13.5	121.5
9	26.25	35.7	8	69.5	13.5	121.5
10	24.1	36.15	9	79	12	108
11	24.9	36.1	11	98	13	117
12	26.3	36.25	11	98	14	126
13	26.8	36.25	11	98	12.5	112.5
14	24.2	36.8	13	117	17.5	157.5
15	25.4	36.6	13	117	16.5	148.5
16	26	36.9	15	136	19.5	175.5
17	27	36.75	13.5	122	19	171
18	28.75	36.75	-	-	15	135
19	23.25	37.3	7.5	64.5	-	-
20	24.9	37.25	16	145.5	21.5	193.5
21	25.25	37.1	18.5	169	25	225
22	26.4	37.4	16	145.5	20	180
23	24.6	37.8	16.5	150	19	171
24	25.75	37.65	18.5	169	19.5	175.5
25	22	37.6	5.5	46	19	171
26	21	38.6	17	155	22	198
27	22	38.5	13	117	17.5	157.5
28	24	38.5	22	202	18	162
29	27.4	38.2	19	174	12	108
30	21.75	39.5	22	202	17	153
31	22.4	39.4	20	183	17	153
32	23.8	39.8	22	202	19	171
33	26.8	39.8	21	192.5	17.5	157.5
34	20.25	40.2	23	211	20	180
35	22.4	40.8	24	220	18.5	166.5
36	24	40.8	-	-	18.5	166.5
37	25.9	40.25	24	220	17	153
38	24.5	41.7	22.5	206.5	19	171
39	26.2	41.7	24	220	19	171

tude) in the forearc, whereas the P receiver functions at the same sites show a reversed velocity contrast (i.e., negative amplitude) (Figure 4). Such a reversal of sign for the Moho conversion has been previously observed by *Bostock et al.* [2002] beneath the Cascadia subduction zone. To obtain a complete picture and examine the origin of the negative amplitude Ps Moho conversion at the forearc stations, we selected and compared P and S receiver functions recorded at four stations (Figure 12); three of them are located in the forearc (SKD, IDI, NPS) and one in continental Greece (PLG). We stack P and S receiver functions and apply a band-pass filter of 4–20 s (Figure 12).

[37] On both the Ps and Sp plots, the bold vector indicates the converted phase from the continental Aegean Moho and the thin vector shows the converted phase from the subducted African Moho. There are no conversions with clear positive amplitude from the Aegean Moho in the P receiver function data at the three forearc stations. Instead, strong converted phases with negative amplitudes appear at delay times of 3–4 s (marked with the bold vectors). Three explanations have been given for the negative amplitude Ps receiver function Moho conversions recorded in Crete. *Knapmeyer and Harjes* [2000] interpret the weak negative signal recorded in western Crete as due to a thick fossil accretionary wedge. *Li et al.* [2003] interpret the negative phase recorded in western and northern central Crete as a reversed Moho velocity contrast caused by a large amount of serpentinite in the mantle wedge. Finally, *Endrun et al.* [2005] conclude that significant Moho topography can provide inverted Moho phases in the forearc.

[38] Considering the results from both the P and S receiver functions, we can discriminate between these different models. Although the Moho converted phases in Figure 12 reveal different polarities for P and S receiver functions at stations located in the forearc, the conversions have the same polarity and arrival time at the station located on mainland Greece. We consider three different crust-mantle contrasts [*Hacker et al.*, 2003] and calculate their corresponding Ps and Sp conversion coefficients (Figure 13). A normal crust overlain by 100% peridotite uppermost mantle shows a positive Ps and a negative Sp conversion coefficient. If the uppermost mantle contains 30% serpentinite, Ps conversion coefficients tend to have smaller

Table 3. Box Number, Coordinate of the Box Center, Measured Delay Times of Sp Conversions From the Aegean Moho and Their Inferred Depths

			Aegean Moho	
Box	Longitude	Latitude	Time, s	Depth, km
1	24.3	34.7	3	25
2	24.2	35.2	2.6	2
3	24.7	35.2	-	-
4	25.25	35.25	3.5	28.5
5	25.6	35.2	2.5	21
6	25.8	35.2	2.8	23
7	26.25	35.25	3.1	25.5
8	24.25	35.6	2	17
9	25.15	35.6	3	25
10	25.2	36.25	3	25
11	25.75	36.2	2.5	21
12	28.3	36.25	2.7	22
13	23.2	36.7	2.7	22
14	24.25	36.75	3	25
15	24.65	36.75	4	33
16	25.2	36.65	3	25
17	25.8	36.8	2.8	23
18	26.7	36.6	3.4	28
19	22.2	37.25	3.5	28.5
20	24.7	37.25	3.5	28.5
21	25.5	37.2	3	25
22	20.7	38.2	4.5	37
23	21.7	38	3	25
24	23.8	38	3.4	28
25	25.5	37.65	3	25
26	27	37.75	3.4	28
27	22	39	3.7	30
28	23.2	38.7	3.4	28
29	23.4	39.4	3.5	28.5
30	26.5	39.25	3.4	28
31	20	39.75	3.9	32
32	21	39.75	3.7	30
33	25.4	40	3.5	28.5
34	22	40.4	3.7	30
35	23.7	40.35	3.5	28.5
36	24	41.25	4	33
37	25.7	41.25	3.5	28.5

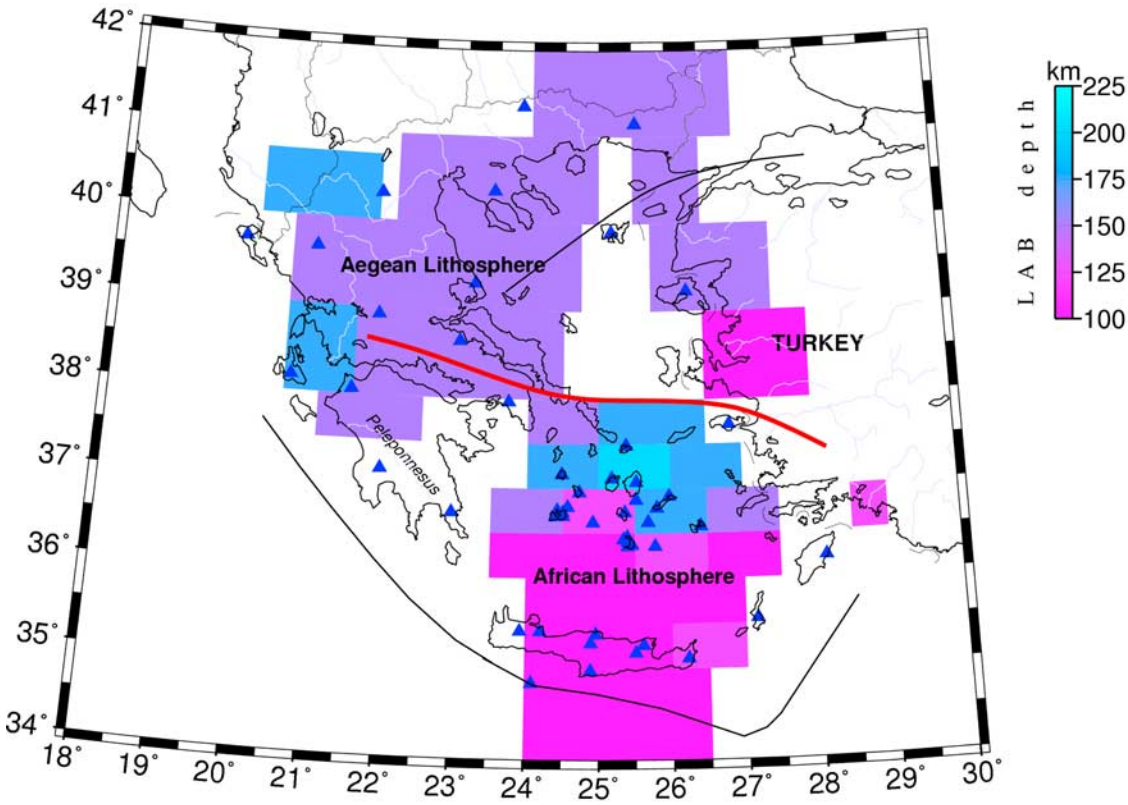

Figure 11. LAB depth map obtained from S receiver function analysis in the Aegean. Time has been converted to depth using the IASP91 reference model. The values are given in Table 2. On the basis of our results, the heavy red line indicates the boundary separating the observed continental Aegean lithosphere from the oceanic African lithosphere.

values, while those of Sp increase. However, for a completely serpentinized uppermost mantle the values of the conversion coefficients are reversed. Ps conversion coefficients become negative and those of Sp are positive. Therefore a large amount of serpentinite (larger than 30%) can provide a negative Ps conversion coefficient leading to a negative amplitude Ps conversion in the forearc. We conclude from our calculations, in contrast to *Knapmeyer and Harjes* [2000] and *Endrun et al.* [2005], and in agreement with *Li et al.* [2003], that greater than 30% serpentinization (~50%) in the forearc upper mantle could result in a negative amplitude P-to-S conversion, while the S-to-P conversion coefficient remains negative.

3.5.2. Topography of the Aegean Moho

[39] We complement the Aegean Moho depth values obtained from P receiver functions (Table 1 and Figure 4) with stacked S receiver functions. Figure 14 shows the distribution of Sp piercing points at 30 km depth (the average depth of the Aegean Moho). By combining both the P and S receiver function results, we can construct a more detailed map of Moho depths for the Aegean area. The Moho depths are evaluated by converting the delay time of the Sp phases into depth using a crustal Vp velocity of 6.2 km/s and a Vp/Vs ratio of 1.73 (Table 3). First, we verify that the Moho depths calculated from P receiver functions beneath each station (Figure 4) agree with the depths computed from stacked S receiver functions for each box encompassing the station (see Figure 14). The time differences between the estimated Ps and Sp converted phases at the Aegean Moho boundary are generally less than 0.4 s (~3 km) and reach 0.7 s (i.e., less than ~6 km in depth) only beneath northwestern Greece. This difference can be caused by the longer period content of the S receiver functions as well as their differing piercing points compared to those of the P receiver functions. Therefore the differences observed between the P and S receiver function Moho conversions are within the expected uncertainties (~5 km). Second, we build a Moho depth map using a relatively homogeneous set of P and S receiver functions measurements. For all stations in the back arc area, we use the Aegean Moho depths calculated from P receiver functions because they are clear and more precise (error ~1.5–2 km). For stations in the forearc region, where no positive Ps converted Moho phase could be determined, we use S receiver functions (error ~5 km). Because of the wider lateral distribution of piercing points for the S receiver functions compared to those of P receiver functions as well as the overlap of S piercing points between neighbor stations (Figure 14), we have improved coverage between stations.

[40] Because of the sparseness of the data recorded at station PENT (24 events) and the large difference in the computed Moho depth relative to its neighboring station ATH (see Figure 1 for station location) and to that computed

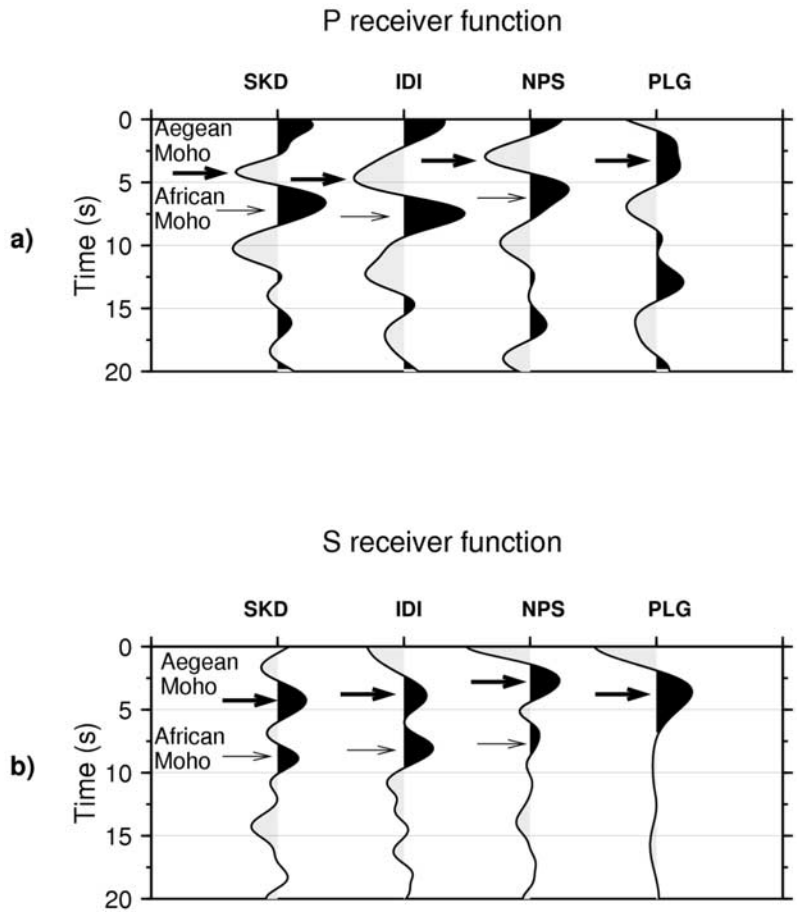

Figure 12. Comparison of P and S receiver functions for 4 selected stations in order to check their compatibility. (a) Stacked P receiver functions show notable negative conversions (bold arrows) at the expected Aegean Moho conversion times at stations in the forearc. This conversion is positive at station PLG on mainland Greece. The interpreted African Moho phase is indicated with thin arrows. (b) Stacked S receiver functions show clear positive conversions at the expected Aegean Moho conversion times for all selected stations. Both types of receiver functions show positive amplitudes for all African Moho phases. Differences in arrival times of the African Moho phases result from the differing lateral locations of the P and S piercing points (see Figure 7).

from S receiver functions in box 24 (see Figure 14), the depth estimate from this station is not used in the Moho map (see also Table 1). For stations MILO and SANT, located on the volcanic islands in the Cyclades region (Figure 1), we observe two similar stable, coherent conversion phases at about 2.5 and 4.5 s (i.e., ~20 and 36 km) in the P receiver functions that arrive within the expected Moho delay time (Figure 15). The observed S receiver functions from box 15 (see Figure 14) including MILO shows a Moho depth of 33 km (~4 s). Therefore we interpret the second phase in the P receiver functions as the Aegean Moho conversion, which reveals a larger amplitude for station SANT. We suspect that the first phase is due to multiple scattering from sediment and upper crustal layers that are commonly present under volcanic islands. Our result confirms the recent work of *Zhu et al.* [2006], which indicates a Moho depth of 33 km at station SANT. *Li et al.* [2003] observed significant energy on the transverse component at station SANT, which correlates well with the converted Moho phase at 4.2 s on the radial component. They interpreted this observation as due to an anisotropic crustal structure. They also showed that the boundary at 25 km depth may be related to the Moho of the Aegean subplate which overlies a thinned remnant of the Cretan microcontinent whose Moho is located at 34 km depth.

[41] Our Aegean Moho depth results are summarized in Figure 16, where all Moho depth estimates are obtained from both P and S receiver functions (Tables 1 and 3). We complemented our results with Moho depth estimates from three stations in Turkey [*Saunders et al.*, 1998]. Furthermore, we have no information on the crustal thickness beneath the central Peloponnesus, which according to geology and gravity anomaly is probably thicker than that of the margin. Therefore we complement our results in this area using the Moho depth values computed by *Tiberi et al.* [2001].

[42] Beneath western Greece the crust is 32–40 km thick. This thick crust is related to isostatic compensation of the Hellenides mountains beneath western part of Greece. Our estimate of the crustal thickness is less than previous studies for this region, where depths were indicated to be ~40–46 km [*Makris*, 1976; *Ligdas and Lees*, 1993; *Papazachos*, 1998;

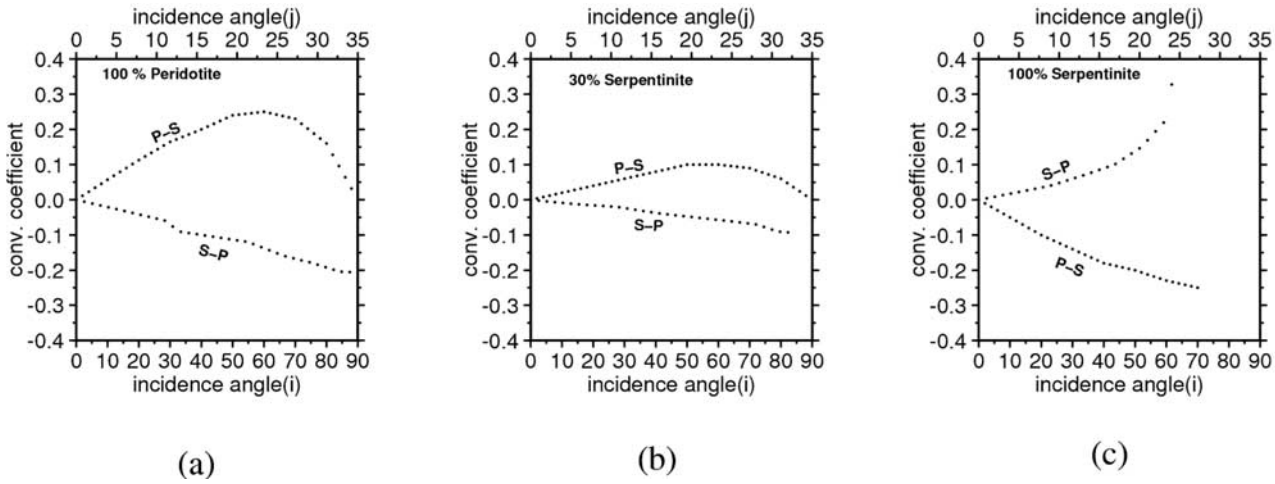

Figure 13. Calculated Ps and Sp conversion coefficients as functions of P wave incidence angle (i) and S wave incidence angle (j), respectively for different models of uppermost mantle materials. (a) Conversion coefficients for a normal crust overlain by 100% peridotite uppermost mantle, (b) uppermost mantle consisting of 30% serpentinite, and (c) completely serpentinized uppermost mantle. Note that in Figure 13c, the values are reversed and Ps conversion coefficients are no longer positive.

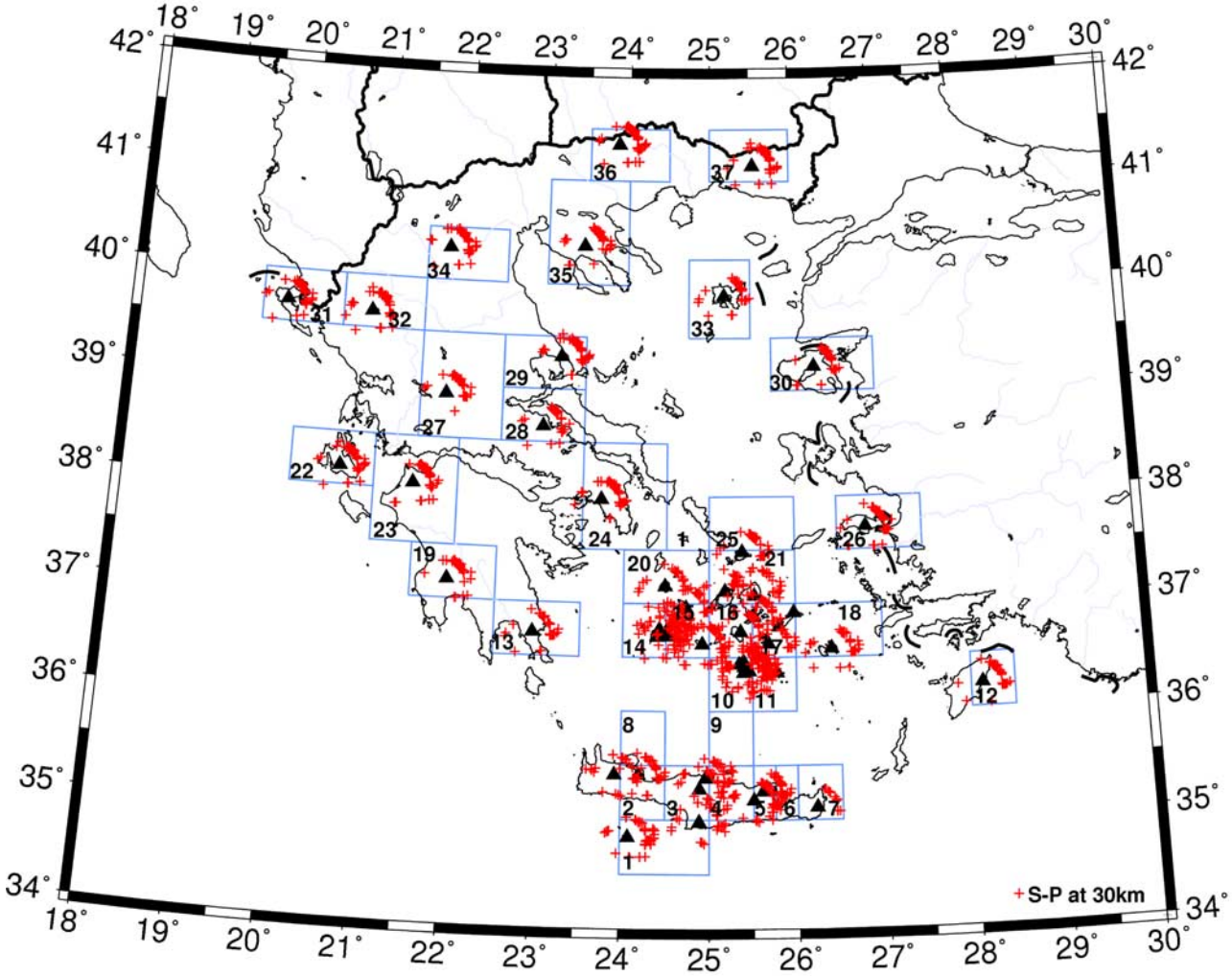

Figure 14. Distribution of Sp conversion points at 30 km depth. The study area is divided into 37 boxes with respect to the location of piercing points at 30 km. The stacked S receiver functions obtained from each box are used to compute the Aegean Moho depth values.

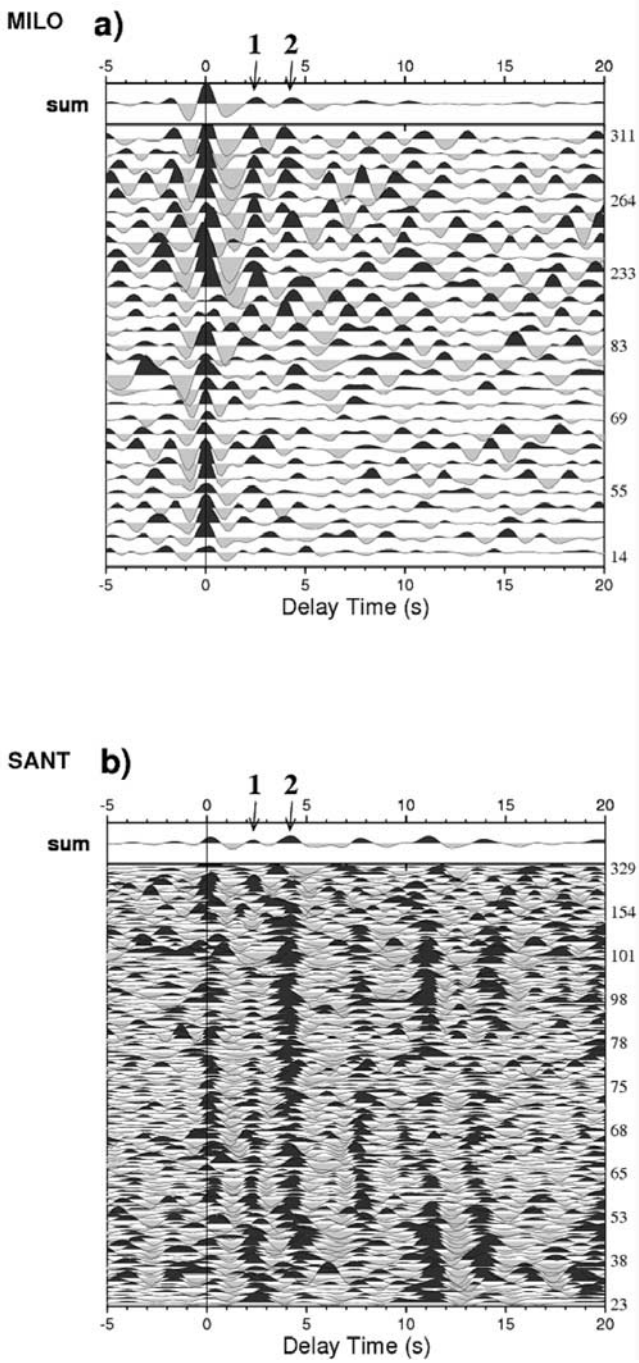

Figure 15. Individual P receiver functions for two stations located on the volcanic islands of Cyclades region, sorted by back azimuth (right legend). The P onset is fixed at zero time. (a) Receiver functions for MILO shows two phases at 2.5 and 4.4 s delay time (labeled 1 and 2, respectively), which give depths of 21 and 36 km, respectively. (b) Receiver functions for SANT show two stable phases at 2.4 and 4.2 s, giving the depths of 19.5 and 34.5 km, respectively. Moho depth obtained from S receiver functions for box 15 (Table 3) including MILO shows a depth of 33 km (~4 s). Thus the phase labeled with 2 is interpreted as the conversion phase from the Aegean Moho.

Tiberi et al., 2000; *Karagianni et al.*, 2002, 2005]. However, these estimates of the Moho depth come from refraction profiles, tomography results and gravity anomalies, which are not appropriate to accurately determine the depth of structural interfaces. On the basis of our results, there is a clear thinning from 40 km at FLOR (see Figure 1 for station location) in the north to 33 km at EVR located in the south and 28 km at JAN located in the western part of Greece. This suggests that the crust is thicker in the center of the Epirus mountains compared to other parts of this area.

[43] Along the west and north coasts of the Aegean Sea, the crust thins to 28–30 km, consistent with the result of *Makris* [1978] for the region of Evia. This thin crust is likely due to the extensional tectonics that affected the whole Aegean and adjacent parts of Greece since the Oligocene time (~30 Myr) as a result of the Hellenic slab southward retreat [e.g., *Gautier and Brun*, 1994]. In the northern Aegean, a region that has undergone crustal extension since the Eocene, the crust is approximately 25–28 km thick. Traveltime [*Papazachos*, 1998] and S wave velocity [*Karagianni et al.*, 2005] tomographic studies also show a relatively thin crust in this area (26–32 km). Wide-angle reflection profiles, conducted in the Sporades Basin (near station SKOP, see Figure 1) show a Moho depth at about 25 km [*Vigner*, 2002]. Beneath the southern Aegean Basin, we observe a very thin crust of about 20–22 km reaching a maximum of 26 km eastward. These results are in good agreement with Moho depths obtained from seismic profiles [*Makris*, 1978; *Bohnhoff et al.*, 2001], shear wave velocity tomography [*Karagianni et al.*, 2005] and receiver function analysis [*van der Meijde et al.*, 2003] for this region. This indicates significant thinning of the crust within this area compared to the northern Aegean area. The contrast between the large-scale present-day thinning associated with the North Aegean Trough, the region with the highest present-day strain rate computed from GPS measurements, and the total thinning inferred from our crustal thickness is consistent with the recent evolution in the geodynamics of the Aegean. This may also imply that if the extension started near the Hellenic trench (the Sea of Crete) during earlier time, it moved away from the trench at roughly the same time as the Hellenic subduction moved southward.

[44] A 26–30 km thick crust is observed beneath the central Aegean across the Cyclades region. This is consistent with earlier refraction data [*Makris*, 1978; *Vigner*, 2002] for this region, which indicated a Moho depth of about 28 km. This thicker crust may suggest that the Cyclades act as a rigid block and hence was not affected by the second episode of the extension, which is mostly concentrated in the northern Aegean Sea [*Tirel et al.*, 2004]. However, the crustal thickness displays a sudden thickening beneath stations MILO and SANT on the volcanic islands where the Moho is 36 and 34 km deep, respectively. This thickening is only related to volcanic islands and does not indicate any relationship with the extensional processes occurring in this area. From our observations we conclude that the average crustal thickness beneath western and central Crete is 30 km and thins to 21–25 km under the eastern part of this island. Our results are in good agreement with the previous results inferred by *Makris* [1978] and *Bohnhoff et al.* [2001] but cannot confirm the results

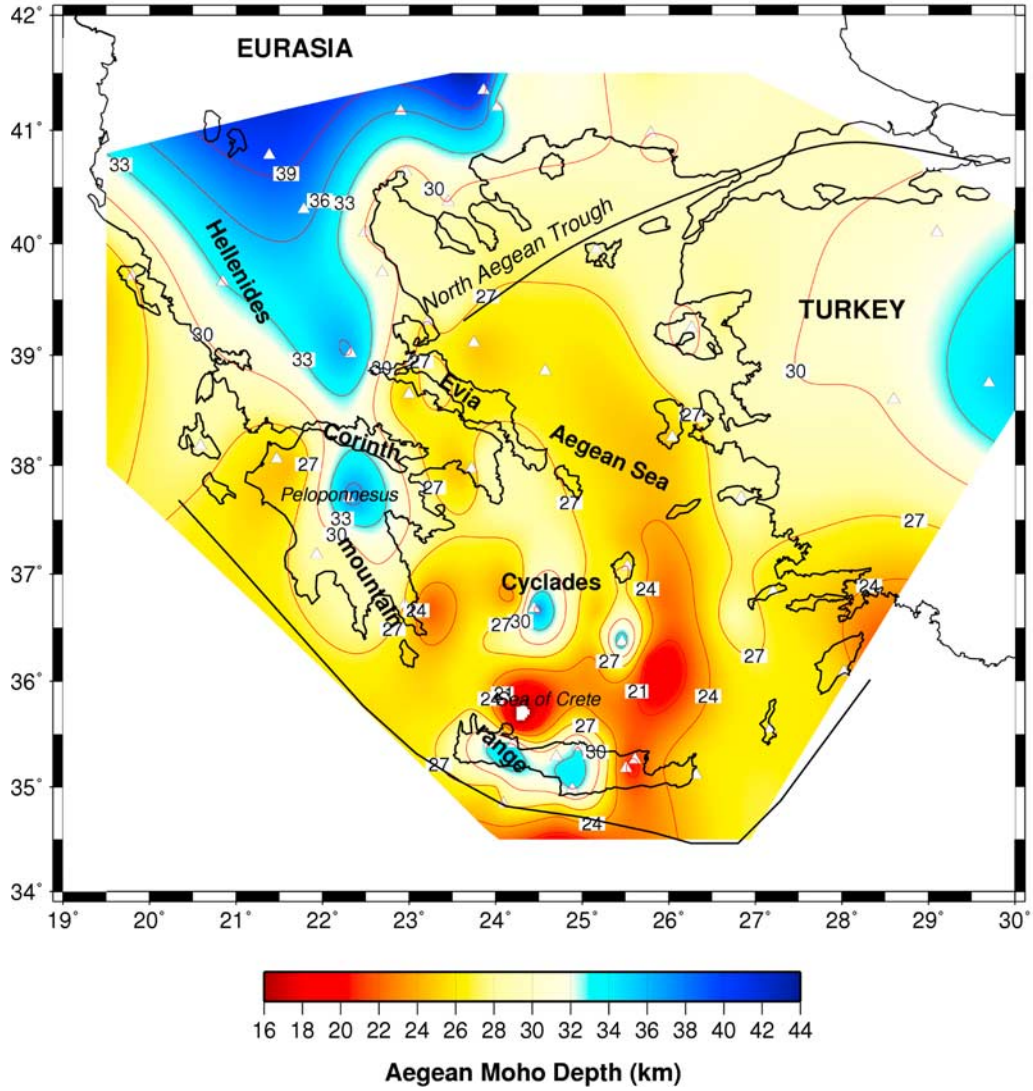

Figure 16. Aegean Moho depth map (in km) obtained from P and S receiver functions. The Moho depth values of three stations in Turkey and one station in the central Peloponnesus are taken from *Saunders et al.* [1998] and *Tiberi et al.* [2001], respectively. The Moho depth values are listed in Tables 1 and 3.

obtained by *Li et al.* [2003] beneath the western part of this island. The difference in the crustal thickness below Crete could be related to the large discontinuity at the surface associated with the Messara basin that results from an horst and graben system that evolved during the Miocene time [*Meulenkamp et al.*, 1988].

[45] On the basis of our results, we infer a thinner crust than previously proposed for the unstretched crust of mainland Greece (32–40 km), and therefore suggest a stretching factor of 20–25% in the northern Aegean and 40–45% in the Cretan Sea. We also find, contrary to previous studies [*Makris*, 1978; *Angelier et al.*, 1982], that low to moderate extension has occurred across the entire Aegean region, which is not restricted only to the Sea of Crete. For the Aegean Sea, our Moho map fits well with gravity anomalies inferred by *Tsokas and Hansen* [1997] and *Tirel et al.* [2004]. However, our Moho map is smoother than what would be expected from surface observations of the topography [*Mascle and Martin*, 1990]. Our Moho estimates reliably show that the continental crust along the Hellenides mountains in the Peloponnesus and Crete has also been partly affected by the extensional processes occurring in the Aegean, consistent with the GPS results in the southern Aegean [*McClusky et al.*, 2000]. We do not observe a NE-SW trend associated with the North Aegean Trough as suggested by the gravity map of *Tirel et al.* [2004]. Indeed, our observations are not very dense (we have measurements only in a few islands) and therefore observe only a smooth Moho topography. Even though this may indicate that the North Aegean Trough is only a superficial feature and does not significantly affect the deeper part of the crust as expected for a lithospheric transtensional fault.

[46] Finally, we suggest that the Moho topography is relatively smooth (25–29 km) in the northern and central Aegean Sea. Large extension in the continental area can result in metamorphic core complexes that are exhumed to the surface from the lower ductile crust. This is the case in

the Aegean [e.g., *Gautier and Brun*, 1994], even though the mechanism of exhumation is still disputed. The Moho topography of the Basin and Range province (another area experiencing large extension) is rather flat [*Gans*, 1987], supporting a model where the lower crust flows to accommodate extension and yield a smooth Moho topography. In the Aegean, our results also show little topography (less than 4 km except beneath the volcanic islands), whereas tectonic observations suggest a larger variability of stretching. This variation is two times less than that proposed by *Zhu et al.* [2006] and, therefore shows a smaller difference in the viscosity of the lower crust between the Basin and Range province and the Aegean area. On the basis of our results, the Aegean and the Basin and Range province show similar variation in Moho topography and so suggests similar mechanical properties for the lower crust.

4. Conclusions

[47] By combining P and S receiver function observations we have obtained a dense seismic sampling of the Aegean Sea and the surrounding regions. We observe a crustal thinning from 38–40 km in western Greece to 28–30 km in the northern and eastern coasts of the Aegean to 25–28 km in the northern Aegean Sea. The discrepancy between the present-day strain rate located mostly in the northern Aegean Sea and the greatest crustal thinning observed beneath the southern Aegean Sea (crustal thickness of 20–22 km) confirms that the present-day kinematic pattern is new. Furthermore, a crustal thickness of 26–30 km beneath the Cyclades in the central Aegean Sea supports this idea, that the second episode of the crustal thinning has not significantly affected this area. The relatively constant Moho depth observed in the northern and central Aegean across the metamorphic complex area suggests that the lower ductile crust compensates the stretching of the upper crust. Observation of the reversed Moho velocity contrast obtained from P receiver functions at forearc stations (Crete, Peloponnesus, Rhodes) indicates serpentinization (~50%) in the mantle wedge of the overriding Aegean plate and is responsible for the reversed sign of the P-to-S conversion coefficient. We found different crustal thicknesses beneath Crete (21–25 km in the east and 30–33 km in the west) and estimate a crustal thickness of 25–28 km beneath the margin of the Peloponnesus.

[48] A high-resolution image of the Hellenic subduction zone demonstrates the penetration of the Moho of the subducting African plate from the Hellenic trench to northern Greece at depths between 40 and 220 km. The shape of the African Moho is coherent with the intermediate seismicity and shows a shallow dip beneath the western Peloponnesus, which becomes steeper beneath Crete and southeast of Rhodes. On the basis of our S receiver functions, the lithosphere-asthenosphere boundary of the subducting African plate is at 100 km depth beneath the southern part of the Aegean region and dips beneath the volcanic arc to a depth of about 225 km and therefore implies a thickness of 60–65 km for the subducted African lithosphere. Beneath western and northern Greece as well as in the northern Aegean Sea, the continental Aegean lithosphere lies above the downgoing African Moho and is observed at about 150 km depth. The thick Eurasian lithosphere, which seems to be smooth across continental Greece and the northern Aegean Sea, suggests that the crust was significantly more involved in the stretching process than the lithosphere. This is associated with the metamorphic core complexes evidenced in the northern Aegean and Cyclades islands.

[49] **Acknowledgments.** The project has been supported by grants from the Deutsche Forschungsgemeinschaft (DFG) by the GFZ Potsdam; the GFZ Geophysical Instrument Pool; the MIDSEA project of ETH Zürich Switzerland; the Bochum University, Germany; the University of Chania, Crete, Greece; the National Observatory of Athens (NOA); and the Seismological Network of the Thessaloniki. Seisfaultgreece was supported by the contract ENV4-CT96-0277 from the program Environment and Climate of the European Commission and by the program IDYL of INSU-CNRS. We thank A. Kirtazi and K. Makropoulos for their invaluable help and observers of both the Geophysical Lab of Thessaloniki and the Geophysical Lab of Athens for their help in the Seisfaultgreece experiment. We also thank Doug Angus for carefully reading the manuscript and helpful comments. Constructive reviews by Meredith Nettles, James Gaherty, and a JGR Associated Editor significantly improved our manuscript.

References

Angelier, J., N. Lyberis, X. Le Pichon, E. Barrier, and P. Huchon (1982), The neotectonic development of the Hellenic arc and the Sea of Crete: A synthesis, *Tectonophysics*, *86*, 159–196.

Armijo, R., B. Meyer, G. King, A. Rigo, and D. Papanastassiou (1996), Quaternary evolution of the Corinth Rift and its applications for the late Cenozoic evolution of the Aegean, *Geophys. J. Int.*, *126*, 11–53.

Bijwaard, H., W. Spakman, and E. R. Engdahl (1998), Closing the gap between regional and global travel time tomography, *J. Geophys. Res.*, *103*, 30,055–30,078.

Bock, G. (1991), Long-period S to P converted waves and the onset of partial melting beneath Oahu, Hawaii, *Geophys. Res. Lett.*, *18*, 869–872.

Bohnhoff, M., J. Makris, D. Papanikolaou, and G. Stravakakis (2001), Crustal investigation of the Hellenic subduction zone using wide aperture seismic data, *Tectonophysics*, *343*, 239–262.

Bostock, M. G., R. D. Hyndman, S. Rondeny, and S. M. Peacock (2002), An inverted continental Moho and serpentinization of the forearc mantle, *Nature*, *417*, 536–538.

Bourova, E., I. Kassaras, H. A. Pedersen, T. Yanovskaya, D. Hatzfeld, and A. Kirtazi (2005), Constraints on absolute S velocities beneath the Aegean Sea from surface wave analysis, *Geophys. J. Int.*, *160*, 1006–1019.

Calcagnile, G., F. D'Ingeo, P. Farrugia, and G. F. Panza (1982), The lithosphere in the central-eastern Mediterranean area, *Pure Appl. Geophys.*, *120*, 389–406.

Christodoulou, A., and D. Hatzfeld (1988), Three-dimensional crustal and upper mantle structure beneath Chalkidiki (northern Greece), *Earth Planet. Sci. Lett.*, *88*, 153–168.

Clément, C., M. Sachpazi, P. Charvis, D. Graindorge, M. Laigle, A. Hirn, and G. Zafiropoulos (2004), Reflection-refraction seismic in the Gulf of Corinth: Hints at deep structure and control of the deep marine basin, *Tectonophysics*, *391*, 97–108.

De Jonge, M. R., M. J. R. Wortel, and W. Spakman (1993), From tectonic reconstruction to upper mantle model: An application to the Alpine-Mediterranean region, *Tectonophysics*, *223*, 53–65.

Delibasis, N., J. Makris, and J. Drakopoulos (1988), Seismic investigation of the crust and the upper mantle in western Greece, *Ann. Geol. Pays Hellen.*, *33*, 69–83.

DeMets, C., R. G. Gordon, D. F. Argus, and S. Stein (1990), Current plate motions, *Geophys. J. Int.*, *101*, 425–478.

Drakatos, G., and J. Drakopoulos (1991), 3-D velocity structure beneath the crust and upper mantle of the Aegean sea region, *Pure Appl. Geophys.*, *135*, 401–420.

Ekström, G., and P. England (1989), Seismic strain rates in regions of distributed continental deformation, *J. Geophys. Res.*, *94*, 10,231–10,257.

Endrun, B., T. Meier, M. Bischoff, and H. P. Harjes (2004), Lithospheric structure in the area of Crete constrained by receiver functions and dispersion analysis of Rayleigh phase velocities, *Geophys. J. Int.*, *158*, 592–608.

Endrun, B., L. Ceranna, T. Meier, M. Bohnhoff, and H. P. Harjes (2005), Modeling the influence of Moho topography on receiver functions: A case study from the central Hellenic subduction zone, *Geophys. Res. Lett.*, *32*, L12311, doi:10.1029/2005GL023066.

Engdahl, E. R., R. van der Hilst, and R. Buland (1988), Global teleseismic earthquake relocation with improved travel times and procedures for depth determination, *Bull. Seismol. Soc. Am.*, *88*, 722–743.

Faber, S., and G. Müller (1980), Sp phases from the transition zone between the upper and lower mantle, *Bull. Seismol. Soc. Am.*, *70*, 487–508.
Farra, V., and L. Vinnik (2000), Upper mantle stratification by P and S receiver functions, *Geophys. J. Int.*, *141*, 699–712.
Gans, P. B. (1987), An open-system, two layer crustal stretching model for the eastern Great Basin, *Tectonics*, *6*, 1–12.
Gautier, P., and J.-P. Brun (1994), Ductile crust exhumation and extensional detachments in the central Aegean (Cyclades and Evia islands), *Geodyn. Acta*, *7*, 57–85.
Hacker, B. R., G. A. Abers, and S. M. Peacock (2003), Subduction factory: 1. Theoretical mineralogy, densities, seismic wave speeds, and H_2O contents, *J. Geophys. Res.*, *108*(B1), 2029, doi:10.1029/2001JB001127.
Hatzfeld, D. (1989), The Hellenic subduction beneath the Peloponnesus: First results of a microearthquake study, *Earth Planet. Sci. Lett.*, *93*, 283–291.
Hatzfeld, D. (1994), On the shape of the subducting slab beneath the Peleponnese, Greece, *Geophys. Res. Lett.*, *21*, 173–176.
Hatzfeld, D., and C. Martin (1992), The Aegean intermediate seismicity defined by ISC data, *Earth Planet. Sci. Lett.*, *113*, 267–275.
Hatzfeld, D., M. Besnard, K. Makropoulos, N. Voulgaris, V. Kouskouna, P. Hatzidimitriou, D. Panagiotopoulos, G. Karakaisis, A. Deschamps, and H. Lyon-Caen (1993), Subcrustal microearthquake seismicity and fault plane solutions beneath the Hellenic arc, *J. Geophys. Res.*, *98*, 9861–9870.
Hatzfeld, D., J. Martinod, G. Bastet, and P. Gautier (1997), An analog experiment for the Aegean to describe the contribution of gravitational potential energy, *J. Geophys. Res.*, *102*, 649–659.
Hatzfeld, D., E. Karagianni, I. Kassaras, A. Kiratzi, E. Louvari, H. Lyon-Caen, K. Makropoulos, P. Papadimitriou, G. Bock, and K. Priestley (2001), Shear wave anisotropy in the upper mantle beneath the Aegean related to internal deformation, *J. Geophys. Res.*, *106*, 30,737–30,753.
Jackson, J. A., and D. P. McKenzie (1988), The relationship between plate motions and seismic moment tensors, and the rates of active deformation in the Mediterranean and Middle East, *Geophys. J.R. Astron. Soc.*, *93*, 45–73.
Jackson, J. A., J. Haines, and W. Holt (1994), A comparison of satellite laser ranging and seismicity data in the Aegean region, *Geophys. Res. Lett.*, *21*, 2849–2852.
Jolivet, L. (2001), A comparison of geodetic and finite strain in the Aegean: Geodynamic implications, *Earth Planet. Sci. Lett.*, *187*, 95–104.
Kahle, H.-G., C. Straub, R. Reilinger, S. McClusky, R. King, K. Hurst, G. Veis, K. Kastens, and P. Cross (1998), The strain field in the eastern Mediterranean region, estimated by repeated GPS measurements, *Tectonophysics*, *294*, 237–252.
Karagianni, E. E., D. G. Pabagiotopoulos, G. F. Panza, P. Suhadolc, C. B. Papazachos, B. C. Papazachos, A. Kirtazi, D. Hatzfeld, K. Makropoulos, K. Priestley, and A. Vuan (2002), Rayleigh wave group velocity tomography in the Aegean area, *Tectonophysics*, *358*, 187–209.
Karagianni, E. E., C. B. Papazachos, D. G. Panagiotopoulos, P. Suhadolc, A. Vuan, and G. F. Panza (2005), Shear velocity structure in the Aegean area obtained by inversion of Rayleigh waves, *Geophys. J. Int.*, *160*, 127–143.
Kennett, B. L. N., and E. R. Engdahl (1991), Travel times for global earthquake location and phase identification, *Geophys. J. Int.*, *105*, 429–465.
Kind, R., and L. P. Vinnik (1988), The upper mantle discontinuities underneath the GRF array from P-to-S converted phases, *J. Geophys.*, *62*, 138–147.
Kissel, C., and C. Laj (1988), The tertiary geodynamical evolution of the Aegean arc; a paleomagnetic reconstruction, *Tectonophysics*, *146*, 183–201.
Knapmeyer, M., and H.-P. Harjes (2000), Imaging crustal discontinuities and the downgoing slab beneath western Crete, *Geophys. J. Int.*, *143*, 1–21.
Kosarev, G., R. Kind, S. V. Sobolev, X. Yuan, W. Hanka, and S. Oreshin (1999), Seismic evidence for a detached Indian lithosphere mantle beneath Tibet, *Science*, *283*, 1306–1309.
Kumar, P., et al. (2005a), The lithosphere-asthenosphere boundary in the north west Atlantic region, *Earth Planet. Sci. Lett.*, *236*, 249–257.
Kumar, P., X. Yuan, R. Kind, and G. Kosarev (2005b), The lithosphere-asthenosphere boundary in the Tien Shan-Karakoram region from S receiver functions: Evidence of continental subduction, *Geophys. Res. Lett.*, *32*, L07305, doi:10.1029/2004GL022291.
Langston, C. A. (1977), The effect of planar dipping structure on source and receiver responses for constant ray parameter, *Bull. Seismol. Soc. Am.*, *67*, 1029–1050.
Le Pichon, X., and J. Angelier (1979), The Hellenic arc and trench system: A key to the neotectonic evolution of the eastern Mediterranean area, *Tectonophysics*, *60*, 1–42.
Le Pichon, X., N. Lyberis, J. Angelier, and V. Renard (1982), Strain distribution over the east Mediterranean ridge: A synthesis incorporating new Sea-Beam data, *Tectonophysics*, *86*, 243–274.
Le Pichon, X., N. Chamot-Rooke, and S. Lallemant (1995), Geodetic determination of the kinematics of central Greece with respect to Europe: Implications for eastern Mediterranean tectonics, *J. Geophys. Res.*, *100*, 12,675–12,690.
Li, X., G. Bock, A. Vafidis, R. Kind, H.-P. Harjes, W. Hanka, K. Wylegalla, M. v. d. Meijde, and X. Yuan (2003), Receiver function study of the Hellenic subduction zone: Imaging crustal thickness variations and the oceanic Moho of the descending African lithosphere, *Geophys. J. Int.*, *155*, 733–748.
Li, X., R. Kind, X. Yuan, I. Wölbern, and W. Hanka (2004), Rejuvenation of the lithosphere by the Hawaiian plume, *Nature*, *427*, 827–829.
Ligdas, C. N., and J. M. Lees (1993), Seismic velocity constrains in the Thessaloniki and Chalkidiki areas (northern Greece) from a 3-D tomographic study, *Tectonophysics*, *228*, 97–121.
Ligdas, C. N., and I. G. Main (1991), On the resolving power of tomographic images in the Aegean area, *Geophys. J. Int.*, *107*, 197–203.
Ligdas, C. N., I. G. Main, and R. D. Adams (1990), 3-D structure of the lithosphere in the Aegean Sea region, *Geophys. J. Int.*, *102*, 219–229.
Makris, J. (1973), Some geophysical aspects of the evolution of the Hellenides, *Bull. Geol. Soc. Greece*, *10*, 206–213.
Makris, J. A. (1976), A dynamic model of the Hellenic arc deduced from geophysical data, *Tectonophysics*, *36*, 339–346.
Makris, J. (1978), The crust and upper mantle structure of the Aegean region from deep soundings, *Tectonophysics*, *46*, 269–284.
Makris, J., and C. Stobbe (1984), Physical properties and state of the crust and upper mantle of the eastern Mediterranean Sea deduced from geophysical data, *Mar. Geol.*, *55*, 347–363.
Makropoulos, K., and P. Burton (1984), Greek tectonics and seismicity, *Tectonophysics*, *106*, 275–304.
Marone, F., M. van der Meijde, S. van der Lee, and D. Giardini (2003), Joint inversion of local, regional and teleseismic data for crustal thickness in the Eurasia-Africa boundary region, *Geophys. J. Int.*, *154*, 499–514.
Mascle, J., and L. Martin (1990), Shallow structure and recent evolution of the Aegean Sea: A synthesis based on continuous reflection profiles, *Mar. Geol.*, *94*, 271–299.
McClusky, S., et al. (2000), Global Positioning System constraints on plate kinematics and dynamics in the eastern Mediterranean and Caucasus, *J. Geophys. Res.*, *105*, 5695–5719.
McKenzie, D. P. (1972), Active tectonics of the Mediterranean region, *Geophys. J.R. Astron. Soc.*, *30*, 109–185.
McKenzie, D. P. (1978), Active tectonics of the Alpine-Himalayan belt: The Aegean Sea and surrounding regions, *Geophys. J.R. Astron. Soc.*, *55*, 217–254.
Mercier, J., D. Sorel, P. Vergely, and K. Simeakis (1989), Extensional tectonic regimes in the Aegean basins during the Cenozoic, *Basin Res.*, *2*, 49–71.
Meulenkamp, J. E., M. J. R. Wortel, W. A. Wamel, W. Spakman, and E. Hoogerduyn Starting (1988), On the Hellenic subduction zone and the geodynamic evolution of Crete since the late middle Miocene, *Tectonophysics*, *146*, 203–215.
Owens, T. J., G. Zandt, and S. R. Taylor (1984), Seismic evidence for an ancient rift beneath the Cumberland Plateau, Tennessee: A detailed analysis of broadband teleseismic P waveforms, *J. Geophys. Res.*, *89*, 7783–7795.
Panagiotopoulos, D. G., and B. C. Papazachos (1985), Travel times of Pn waves in the Aegean and surrounding area, *Geophys. J.R. Astron. Soc.*, *80*, 165–176.
Papazachos, B. C. (1969), Phase velocities of Rayleigh waves in the southeastern Europe and eastern Mediterranean Sea, *Pure Appl. Geophys.*, *75*, 47–55.
Papazachos, B. C. (1990), Seismicity of the Aegean and surrounding area, *Tectonophysics*, *178*, 287–308.
Papazachos, B. C., and P. E. Comninakis (1969), Geophysical features of the Greek Island arc and eastern Mediterranean ridge, *C.R. Seances Conf. Reunie Madrid*, *16*, 74–75.
Papazachos, B. C., and P. E. Comninakis (1971), Geophysical and tectonic features of the Aegean arc, *J. Geophys. Res.*, *76*, 8517–8533.
Papazachos, B. C., V. G. Karakostas, C. B. Papazachos, and E. M. Scordilis (2000), The geometry of the Wadati-Benioff zone and lithospheric kinematics in the Hellenic arc, *Tectonophysics*, *319*, 275–300.
Papazachos, C. B. (1998), Crustal and upper mantle P and S velocity structure of the Serbomacedonian massif (northern Greece), *Geophys. J. Lett.*, *134*, 25–39.
Papazachos, C. B., and G. Nolet (1997), P and S deep velocity structure of the Hellenic area obtained by robust nonlinear inversion of travel times, *J. Geophys. Res.*, *102*, 8349–8367.
Papazachos, C. B., P. M. Hatzidimitriou, D. G. Panagiotopoulos, and G. N. Tsokas (1995), Tomography of the crust and upper mantle in southeast Europe, *J. Geophys. Res.*, *100*, 12,405–12,422.

Payo, G. (1967), Crustal structure of the Mediterranean Sea by surface waves, I, Group velocity, *Bull. Seismol. Soc. Am.*, *57*, 151–172.

Payo, G. (1969), Crustal structure of the Mediterranean Sea by surface waves, II, Phase velocity and travel time, *Bull. Seismol. Soc. Am.*, *59*, 23–42.

Reilinger, R., S. McClusky, M. B. Oral, R. W. King, and M. N. Toksoz (1997), Global Positioning System measurements of present-day crustal movements in the Arabia-Africa-Eurasia plate collision zone, *J. Geophys. Res.*, *102*, 9983–9999.

Saunders, P., K. Priestley, and T. Taymaz (1998), Variations in the crustal structure beneath western Turkey, *Geophys. J. Int.*, *134*, 373–389.

Sodoudi, F., X. Yuan, Q. Liu, R. Kind, and J. Chen (2006), Lithospheric thickness beneath the Dabie Shan, central eastern China from S reciever functions, *Geophys. J. Int.*, *166*, 1363–1367.

Sorel, D., J. L. Mercier, B. Keraudren, and M. Cushing (1988), Le rule de la traction de la lithosphere subductèe dans l'Èvolution gèodynamique Plio-Pleistocene de l'arc Ègèen: mouvement verticaux alternès et variations du règime tectonique, *C.R. Acad. Sci.*, *307*, 1981–1986.

Spakman, W. (1986), Subduction beneath Eurasia in connection with the Mesozoic Tethys, *Geol. Mijnbouw.*, *65*, 145–153.

Spakman, W., M. J. R. Wortel, and N. S. Vlaar (1988), The Hellenic subduction zone: A tomographic image and its geodynamical implications, *Geophys. Res. Lett.*, *15*, 60–63.

Spakman, W., S. Van der Lee, and R. D. Van der Hilst (1993), Travel time tomography of the European-Mediterranean mantle down to 1400 km, *Geophys. Res. Lett.*, *15*, 60–63.

Taymaz, T., J. A. Jackson, and D. McKenzie (1991), Active tectonics of the north and central Aegean Sea, *Geophys. J. Int.*, *106*, 433–490.

Tiberi, C., H. Lyon-Caen, D. Hatzfeld, U. Achauer, E. Karagianni, A. Kirtazi, E. Louvari, D. Panagiotopoulos, I. Kassaras, G. Kaviris, K. Makropoulos, and P. Papadimitriou (2000), Crustal and upper mantle structure beneath the Corinth rift (Greece) from a teleseismic tomography study, *J. Geophys. Res.*, *105*, 28,159–28,172.

Tiberi, C., M. Diament, H. Lyon-Caen, and T. King (2001), Moho topography beneath the Corinth Rift area (Greece) from inversion of gravity data, *Geophys. J. Int.*, *145*, 797–808.

Tirel, C., F. Gueydan, C. Tiberi, and J.-P. Brun (2004), Aegean crustal thickness inferred from gravity inversion Geodynamical implications, *Earth Planet. Sci. Lett.*, *228*, 267–280.

Tsokas, G. N., and R. O. Hansen (1997), Study of the crustal thickness and subducting lithosphere in Greece from gravity data, *J. Geophys. Res.*, *102*, 20,585–20,597.

van der Meijde, M., S. van der Lee, and D. Giardini (2003), Crustal structure beneath broad-band seismic stations in the Mediterranean region, *Geophys. J. Int.*, *152*, 729–739.

Vigner, A. (2002), Images sismiques par reflexions verticale et grand-angle de la croute en contexte extensif, Les Cyclades et le Fosse Nord-Egeen, these, 269 pp., Inst. Phys. du Globe de Paris, Paris.

Wortel, M. J. R., S. D. B. Goes, and W. Spakman (1990), Structure and seismicity of the Aegean subduction zone, *Terra Nova*, *2*, 554–562.

Wortel, R. (1982), Seismicity and rheology of subducted slabs, *Nature*, *296*, 553–556.

Yuan, X., S. V. Sobolev, and R. Kind (2002), Moho topography in the central Andes and its geodynamic implication, *Earth Planet. Sci. Lett.*, *199*, 389–402.

Yuan, X., R. Kind, X. Li, and R. Wang (2006), The S receiver functions: Synthetics and data example, *Geophys. J. Int.*, *165*, 555–564.

Zandt, G., and C. J. Ammon (1995), Continental crust composition constrained by measurements of crustal Poisson's ratio, *Nature*, *374*, 152–154.

Zhu, L., and H. Kanamori (2000), Moho depth variation in southern California from teleseismic receiver functions, *J. Geophys. Res.*, *105*, 2890–2969.

Zhu, L., B. J. Mitchell, N. Akyol, I. Cemen, and K. Kekovali (2006), Crustal thickness variations in the Aegean region and implications for the extension of continental crust, *J. Geophys. Res.*, *111*, B01301, doi:10.1029/2005JB003770.

M. Bohnhoff, GeoForschungsZentrum Potsdam, Telegrafenberg, 14473 Potsdam, Germany.

W. Hanka, R. Kind, F. Sodoudi, and K. Wylegalla, GeoForschungsZentrum Potsdam, Telegrafenberg, D-14473 Potsdam, Germany. (foroug@gfz-potsdam.de)

H.-P. Harjes, Department of Geosciences, Ruhr-University Bochum, D-44780 Bochum, Germany.

D. Hatzfeld, Laboratoire des Geophysique Interne et Tectonophysique, 1381, rue de la Piscine, F- 38041 Grenoble Cedex 9, France.

K. Priestley, Bullard Laboratory, Madingley Rise, Cambridge CB3 0EZ, UK.

G. Stavrakakis, National Observatory of Athens, P.O. Box 20048, GR-11810 Athens, Greece.

A. Vafidis, Department of Mineral Resources Engineering, Technical University of Chania, GR-73100 Chania, Crete, Greece.